# Advanced numerical models for the analysis of masonry cross vaults: A case-study in Italy

Gabriele Milani [a,*], Michele Simoni [b], Antonio Tralli [b]

[a] Department of Architecture, Built Environment and Construction Engineering (A.B.C.), Technical University in Milan, Piazza Leonardo da Vinci 32, 20133 Milan, Italy
[b] Department of Engineering, University of Ferrara, Via Saragat 1, 44100 Ferrara, Italy

*Article history:*
Received 26 December 2013
Revised 14 June 2014
Accepted 15 July 2014
Available online 8 August 2014

## 1. Introduction

The analysis of masonry vaults under both gravity loads and horizontal seismic action is still an open issue that deserves great consideration by specialized technicians.

Double curvature masonry structures in the form of arches, bridges, cross vaults and cupolas constitute a considerable percentage of the historical built heritage: for this reason, their study – mainly based on graphical statics – goes back to the early 18th century. Among the others, the approaches based on 1D equilibrium equations for the study of masonry domes and proposed by Bouguer (1734), Coulomb (1773), Bossut (1778) and Mascheroni (1785), are worth noting.

Anyway, what was clear from the beginning, was that non-linearity appears very early on curved masonry elements, even in presence of self-weight and with very low tensile stresses.

Taking into account such important feature, a considerable improvement in the analysis of spherical domes was achieved when Levy (1888) proposed a graphical analysis aimed at finding the circle on which circumferential forces vanish. For an exhaustive history of the theories of masonry vaults we refer the reader to the comprehensive treatise by Benvenuto [1].

Exception made for some particular cases either where geometric and load symmetry may help in simplifying the problem or for single curvature structures (arches), and despite the considerable wide spreading of Finite Elements programs, it can be affirmed that, at present the models available to practitioners for a fast and reliable analysis of curved structural elements beyond the elastic limit are a few, see for instance the indications provided by Como [2], Paradiso and Tempesta [3], Mark et al. [4], Heyman [5–7] and Huerta [8].

Limit analysis theorems associated with FEs, both in the static and kinematic version, are still the most effective and widespread procedure to estimate the collapse loads of one dimensional arches [9–14]. In a similar way, cupolas may be treated as well, but only under the quite restrictive condition of axi-symmetric loads

* Corresponding author. Tel.: +39 022399 4290; fax: +39 022399 4220.
*E-mail address:* milani@stru.polimi.it (G. Milani).

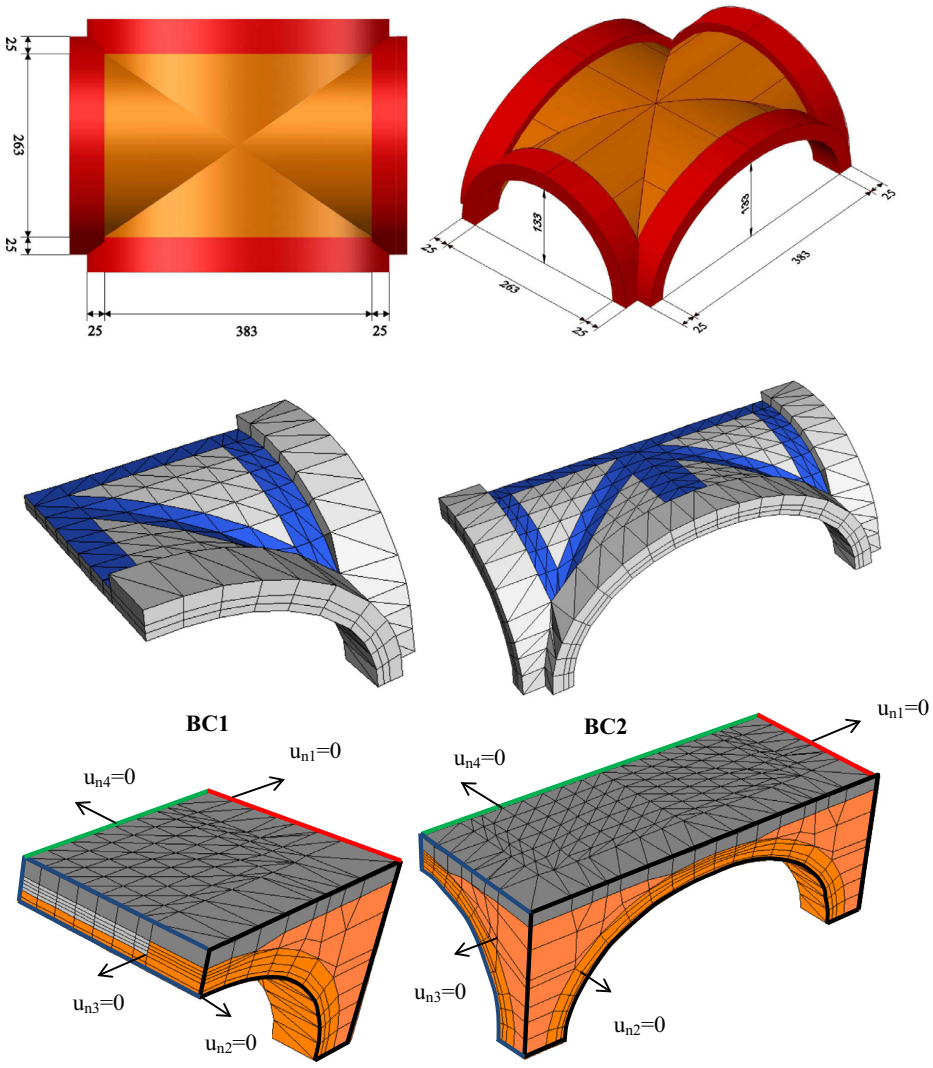


**Fig. 1.** Top, plan and perspective view of the rectangular cross vault analyzed (dimensions in centimeters). Center, first and second boundary condition configurations BC1 & BC2 without infill, FE discretization. Bottom, first and second boundary condition configurations BC1 & BC2 with infill.

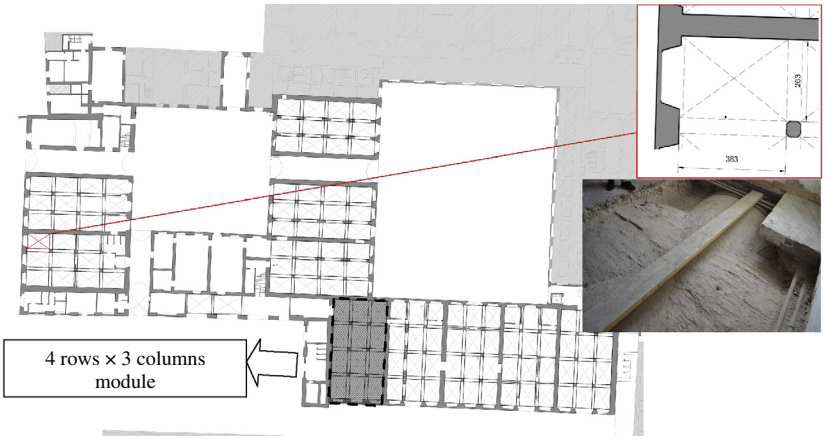


**Fig. 2.** Ground floor planar view with identification of the position of the vaults.

[14–17]. Exception made for some special cases, the extension of automated approaches for complex geometries, general load conditions, reinforced arches and structures interacting with the infill still remains a challenging topic [18–22], despite experimentation in the field is putting at disposal a huge amount of experiences and evidences [23–25]. In absence of dedicated software, the most

**Fig. 3.** Existing state of damage. Diagonal cracks (top) and full detachment of the lateral ribbed arch (bottom).

**Table 1**
Rectangular cross vault in Lucca, mechanical properties adopted in the numerical simulations.

| | | | |
|---|---|---|---|
| *Masonry* | | | |
| $E$ | 1500 | (MPa) | Young Modulus |
| $G$ | 500 | (MPa) | Shear Modulus |
| $c$ | $1.2f_t$ | (MPa) | Cohesion |
| $f_t$ | 0.05–0.1–0.15–0.2 | (MPa) | Tensile strength |
| $f_{ce}$ | $1/3f_{cp}$ | (MPa) | Compressive hardening/softening behavior |
| $f_{cp}$ | 2.4 | (MPa) | |
| $f_{cm}$ | $0.8f_{cp}$ | (MPa) | |
| $f_{cr}$ | $0.5f_{cp}$ | (MPa) | |
| $\varepsilon_p$ | $5\varepsilon_{el}$ | (–) | |
| $\kappa_m$ | $10\varepsilon_{el}$ | (–) | |
| $\Phi$ | 30 | (°) | Friction angle |
| $Y$ | 45 | (°) | Angle of the linearized compressive cap |
| $G_f^{\mathrm{I}}$ | 0.005–0.010–0.015–0.020 | (N/mm) | Mode I fracture energy |
| $G_f^{\mathrm{II}}$ | $4/5G_f^{\mathrm{I}}$ | (N/mm) | Mode II fracture energy |
| *Infill* | | | |
| $E$ | 750 | (MPa)) | Young Modulus |
| $G$ | $E/2$ | (MPa) | Shear Modulus |
| $c$ | $1.0f_t$ | (MPa) | Cohesion |
| $f_t$ | 0.01–0.015–0.02–0.025 | (MPa) | Tensile strength |
| $\Phi$ | 37 | (°) | Friction angle |

straightforward approach still remains the utilization of non-linear FEs either already implemented in commercial codes [26,27] or non commercial but conceived for isotropic materials, as for instance concrete [21,22].

The authors have been active in this field from many years and recently proposed several different approaches for a fast and reliable analysis up to collapse of masonry vaults which take into account several distinctive aspects of the material, as orthotropy

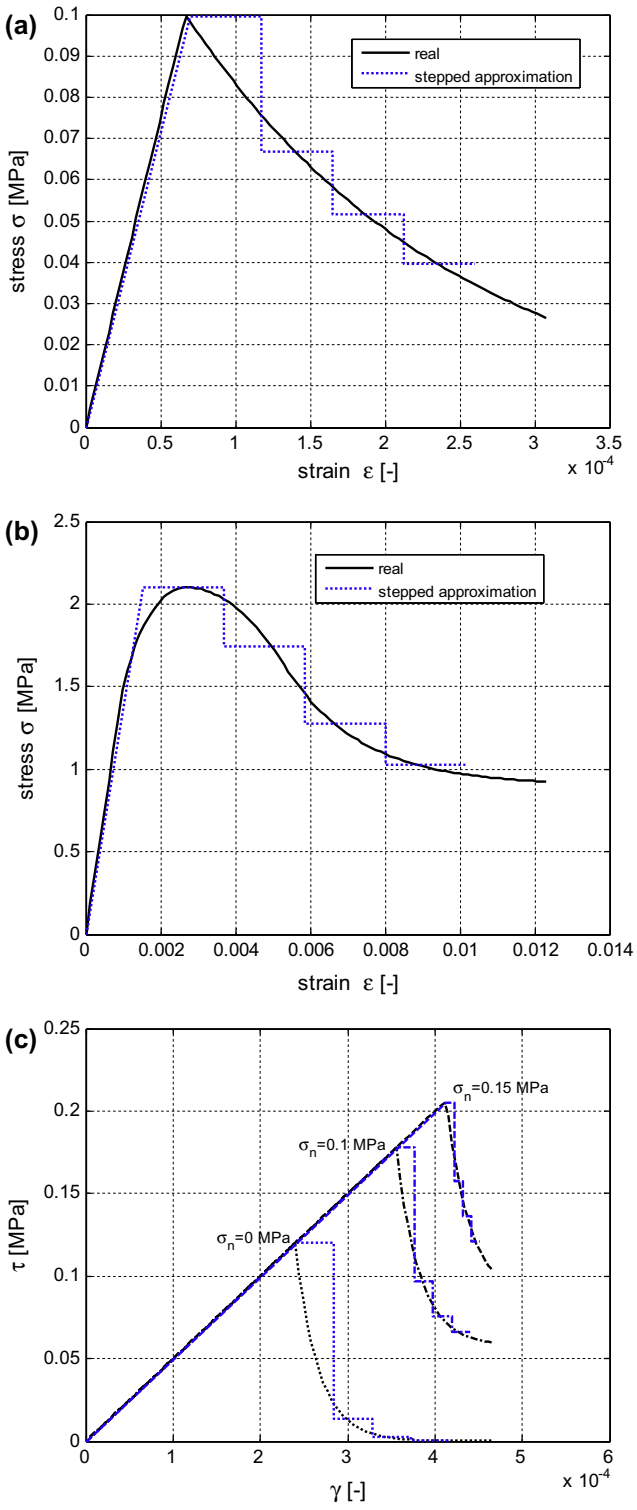


**Fig. 4.** Arch stress strain curves used in the non-standard FE approach proposed and their approximation by means of linear-piecewise constant functions. (a): tension, (b): comression and (c) shear.

and finite ductility [28–33]. The models include (1) homogenized limit analyses by means of both plate and shell [33] and 3D elements [31,32] and (2) incremental non-linear approach with rigid wedge elements and homogenized non-linear interfaces [28,29].

An enhanced code [30] recently presented allows the possibility to model FRP reinforcement strips and steel tie rods, to

**Fig. 5.** Photo of the infill clearly demonstrating the very low cohesion.

quantitatively compare the situation before and after a rehabilitation intervention conducted with either innovative or traditional technology, thus implicitly selecting the most effective strategy for structural upgrading and refurbishment.

Object of the present study is the structural analysis of a series of existing masonry cross vaults constituting the roof system of the ground floor of the former Caserma Lorenzini in Lucca, Italy, at the moment subjected to a wide restoration intervention within the so called PIUSS project, aimed at the urban renewal of the area and at a change of destination use of the building, which will host the Italian National Comics museum and a nursery school.

The vaults system covers a large area with irregular shape by means of rectangular modules of dimension roughly equal to 17.30 × 7.40 m, further constituted by a 4 rows and 3 columns regular grid in plan of vaults. A single vault has a dimension in plan equal to 3.13 × 4.33 m, see Fig. 1, whereas modules disposition is as in Fig. 2.

Generally, the vaults exhibit a visible state of degradation, with frequent passing cracks on boundary and diagonal arches.

The analysis of a cross vault with a series of arches, commonly employed by practitioners [2–8], whilst very attractive for its simplicity, remains theoretically questionable, because it does not take into account the actual biaxial state of stress acting on the crossing barrel vaults. As it is shown in the present paper, sometimes it provides results not sufficiently in agreement with more sophisticated analyses, as those used in this paper, and is unable to reproduce some typical damage patters that traditionally are observed on vaulted systems, as for instance Sabouret's cracks [19,21,22], which spread at the intersection between the vault and the boundary arches (as it occurs in the present case study).

Another important aspect that has to be taken into account is to quantitatively have an insight into the role played by the infill. As well known, infill may have a beneficial role [28,34–37], but usually this aspect is taken into account in common software only in an approximate way adding a fictitious stabilizing horizontal pressure on the abutments. Cavicchi and Gambarotta [36,37] were probably the first to rigorously take into account infill by means of its discretization with plane triangular elements within a FE upper bound limit analysis procedure. Such approach, extended recently to 3D bridges [28], requires however dedicated software not available on the market and a generalization to the 3D case for masonry cross vaults.

In the present paper, different advanced numerical strategies under different load, constrain and material properties conditions, are adopted to analyze a typical cross vault belonging to the

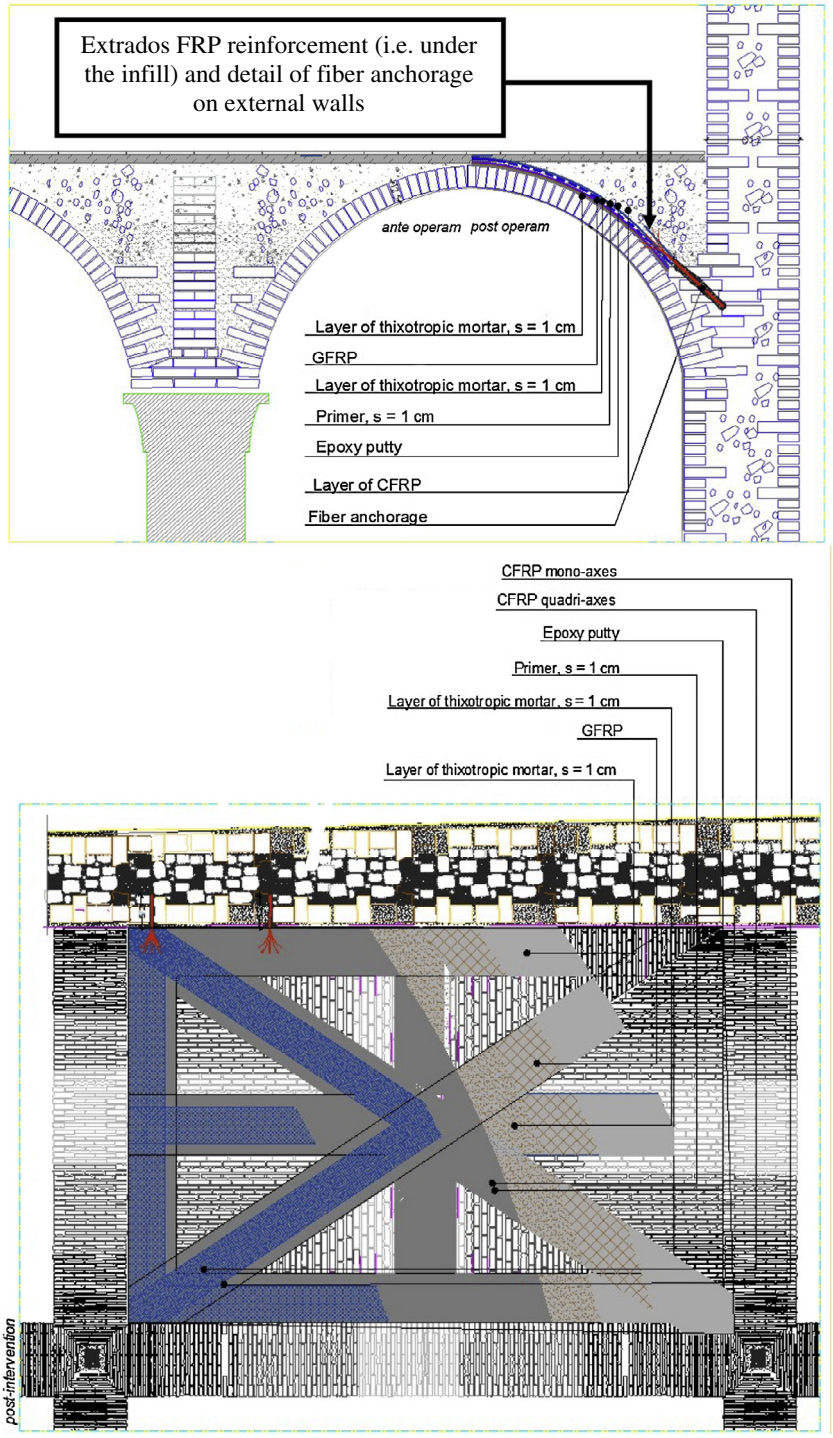


**Fig. 6.** Extrados FRP reinforcement, transversal section and planar view.

building under consideration. The analyses include limit and non-linear static approaches conducted by means of non-commercial software and a simplified approach by means of the subdivision of the cross vault into single arches. To study the single arch, a Matlab implementation of a software based on the evaluation of the thrust line has been developed.

The vaults are analyzed before and after a rehabilitation intervention made with carbon fibers, in order to evaluate (1) if the structure is safe under vertical loads, (2) what is the increase of the load bearing capacity due to the infill, (3) what is the efficacy of the rehabilitation intervention and the associated increase of the load bearing capacity obtained.

The paper is organized as follows: in Section 2 the geometry and mechanical properties of the vaulted systems are presented, in Section 3 the numerical models employed, previously developed by the Authors, are briefly overviewed, finally in Section 4 the results of the numerical simulations are presented and critically discussed in detail.

## 2. Geometry and mechanical properties of the vaulted system

The vaults system covers a ground floor of a large building with irregular shape in plan, see Fig. 2. In total, 108 single cross vaults are present, disposed in interesting rectangular blocks constituted by 4 rows and 3 columns of vaults. The 108 vaults are geometrically almost identical, exception made for the constraint conditions of the lateral vaults when compared with the central ones.

The dimension in plan of each single vault is 313 × 433 cm, see Fig. 1. The vault is approximately 12 cm thick and is constituted by a single brick along the thickness. Common traditional Italian clay bricks are utilized (dimensions $12 \times 5.5 \times 25\ mm^3$, thickness × height × length) disposed with their height along the direction of the barrel vault with non-null curvature (blocks disposition is as in Fig. 3). Four ribbing arches having thickness equal to 25 cm are present, externally bounding the structure, whereas the cross arches are not ribbed.

Exception made for some localized superficial detachment of material in correspondence of the joints, a sufficient level of conservation is observed, as well as the visual quality of the material under consideration.

Apart a quite classic damage pattern, represented by Sabouret's cracks, propagating parallel to geometric principal axes of the vault, at the interface between the vault and the boundary arches, unusual cracks along both diagonals are observed, see Fig. 3, probably a consequence of the absence of intrados ribbing arches.

According to Italian Code NTC 2008 [38], Chapter 8, and subsequent Explicative Notes 2009 [39], the mechanical properties to assume for the masonry material depend on the so called knowledge level LC, which is related to the so called Confidence Factor Fc. The Italian code provides three different LCs, labeled from 1 to 3, related to the level of knowledge that one has on the mechanical and geometrical properties of the structure. LC3 corresponds to a very detailed survey, i.e. where also in-situ and laboratory tests on extracted samples are performed, whereas LC1 is linked to the less detailed survey, which includes visual inspection and geometric survey. For the case at hand, in absence of specific in-situ test results, a LC1 level is assumed.

Fc is a coefficient that accounts for the level of knowledge regarding the structure and the foundation system, from a geometric and mechanical point of view. It can be determined defining different partial confidence factors $F_{Ck}$ ($k$ = 1,4), on the base of some numerical coefficients present in the Italian Code (Table 4.1 Italian Line Guides). Due to the limited level of knowledge achieved in this case, the highest confidence factor was used, FC = 1.35.

After visual inspections, values adopted for cohesion and masonry elastic moduli are taken in agreement with Table C8A.2.1 Explicative Notes 2009 [39], assuming a masonry typology constituted by clay bricks with very poor mechanical properties of the joint and quite regular courses.

Elastic and inelastic material properties utilized in all the analyses for the arches are reported in Table 1. With the lowest knowledge level LC (confidence factor $F_C$ = 1.35), Italian code safely requires to select in Table C8A.2.1, the lower bound values for strength and the average between lower and upper bound for elastic moduli.

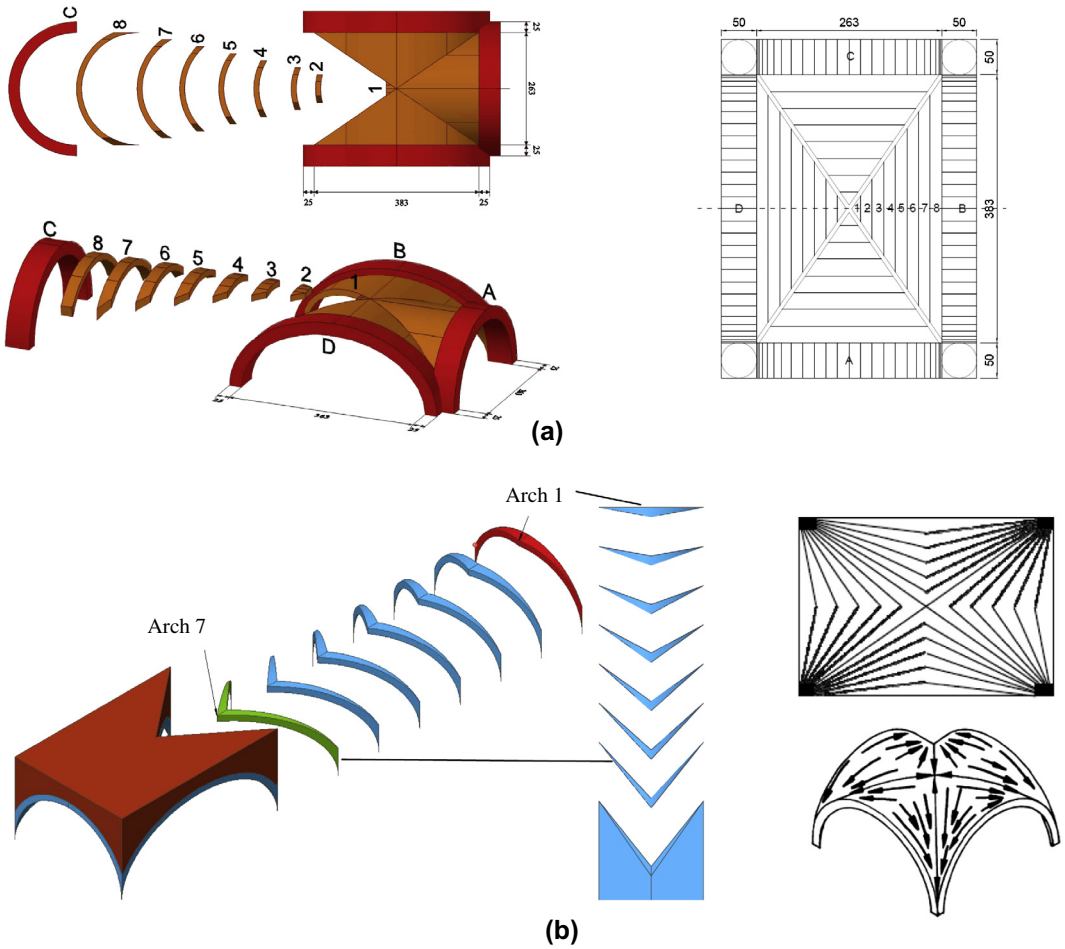


**Fig. 7.** (a) Straight decomposition of the vault into several single curvature arches [2,3]. (b) Alternative non straight decomposition into arches following observed photoelastic membrane forces flux [4].

## 3. Brief overview of the numerical models utilized

Three distinct numerical approaches are utilized in the paper: (1) a simplified approach by means of the analysis of a single vault regarded as the assemblage of separated arches [2], (2) a homogenized limit analysis conducted with 3D elements and [31–33] (3) a non-linear homogenized procedure by means of a Quadratic Programming procedure recently presented by the authors in [29].

It is interesting to comparatively evaluate the results provided by the different approaches and to eventually identify univocally the reasons at the base of the state of damage of the structures.

In what follows a very brief overview of the three distinct procedures proposed is discussed, putting in evidence the simplifications introduced in the different procedures, limits of applicability and weakness points.

### *3.1. Decomposition of the cross vaults into single curvature arches*

A classic method to the simplified analysis of masonry cross vaults is that proposed by Como [2], who suggested decomposing the vault in many parallel arches, see Fig. 7-a. Each arch is then analyzed determining the thrust line under the external loads assigned, provided that the following hypotheses (Heyman [5–7]) are made for masonry: (1) the material is supposed unable to withstand tensile stresses, (2) an infinite compressive strength is assumed and (3) shear sliding of contiguous blocks is not allowed. Implicitly, the third hypothesis requires that each arch fails for the formation of a sufficient number of flexural hinges forming an active failure mechanism.

The approach neglects the mutual interaction between contiguous arches and therefore may be considered as a "safe" procedure. The arches along the diagonals, whilst not ribbed, are also considered and loaded by means of the reactions of the arches disposed in plan along the edges. On each single arch, external loads (including infill) and self-weight act.

The possibility to deal with the role played by the infill in the stability of each single arch is still possible in an approximate way, following the procedure used for instance within Ring software by Gilbert and co-workers [40–42], who add a stabilizing horizontal pressure depending on the infill weight multiplied by a coefficient of horizontal retention $K_h$.

A second simplified approach proposed in the literature [14] and derived from the observation of the internal stress distribution during photo-elastic tests [4] is also considered. Such procedure is based on an alternative decomposition that proved to perform well especially for Gothic vaults with weak diagonal arches, see Fig. 7-b.

In such decomposition by means of non-straight arches, the membrane is the critical member, while the diagonal arches (or cross ribs) do not work. Thus the cross section combination is generally diagonal to the main axes of the vault, in a way to follow the force trajectories.

It is worth noting however that, in the safety assessment used within the PIUSS project, the first decomposition model (implemented also in the commercial code Aedes [3]) was adopted and no mention is given to the second approach, which is discussed here only to have an insight into its real capability of providing reasonable results in this particular case.

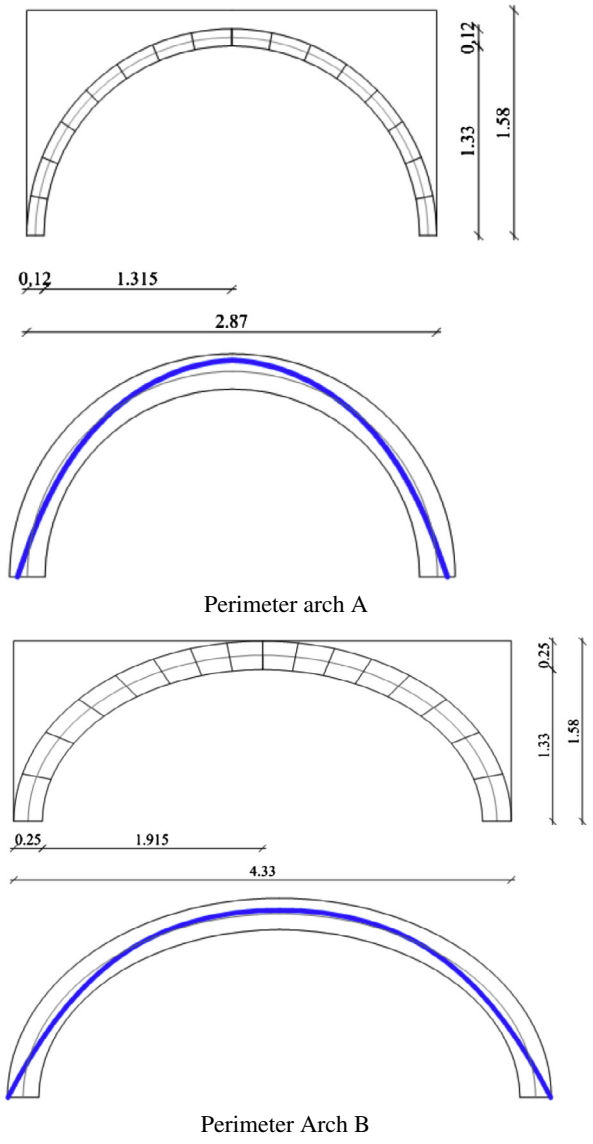


**Fig. 8.** Results from the traditional thrust lines analysis of the lateral elliptic arch and the frontal circular arch.

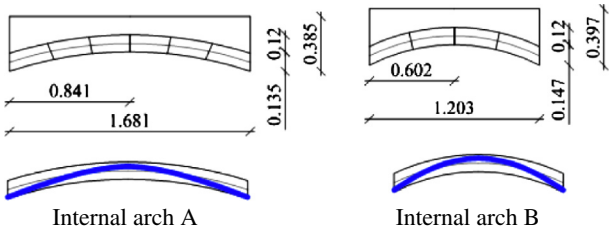


**Fig. 9.** Results from the traditional analysis, thrust lines of the internal arches, Internal arch A & B.

### *3.2. Homogenized limit and step-by-step non-linear analyses*

In both the limit and step-by step non-linear models, a homogenization approach is used, meaning that the vault is modeled by means of an orthotropic homogenized material obtained with a mesoscopic approach similar to that proposed in [43–46], whereas infill is modeled by means of an isotropic Mohr–Coulomb material with tension cutoff and softening.

Both the limit and the non-linear analysis require a structural implementation with discretization of masonry and infill with six-noded rigid infinitely resistant wedge shaped elements.

In this way, all deformation is concentrated exclusively on interfaces (modeled assuming either an isotropic frictional material as for the backfill or by means of a homogenized orthotropic

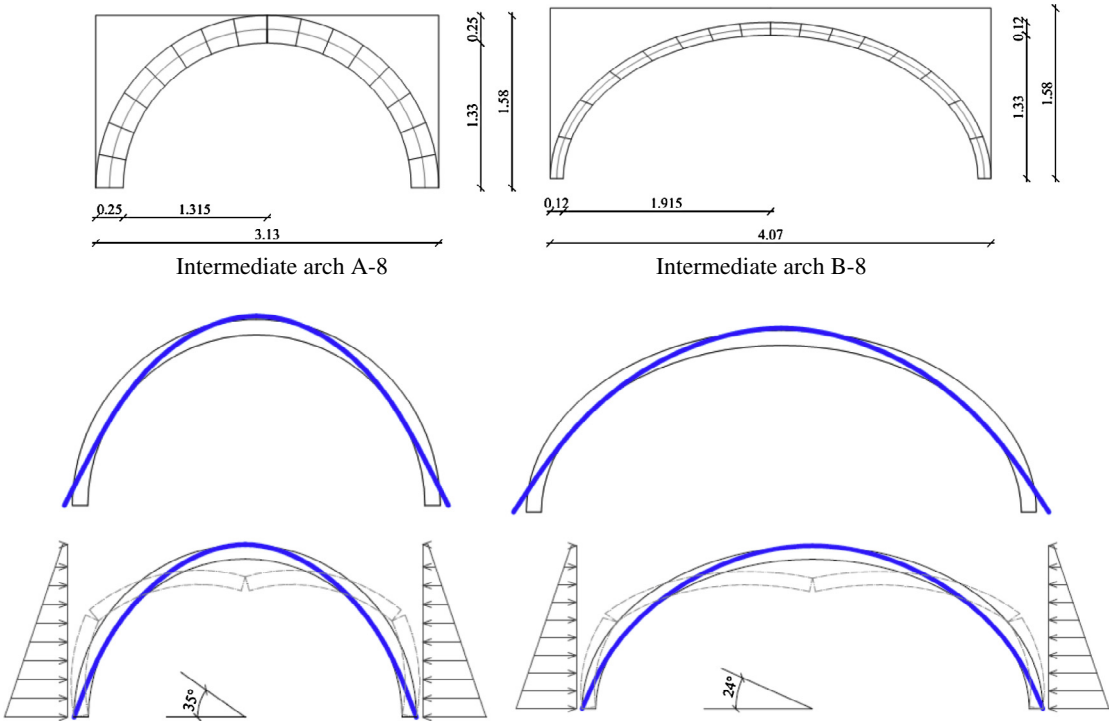


**Fig. 10.** Results from the traditional analysis, thrust lines of the internal arches and kinematic limit analysis, intermediate arch A & B.

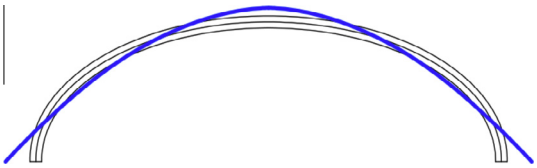

**Fig. 11.** Results from the traditional analysis, diagonal arch.

material as in case of masonry), thus requiring a very limited number of optimization variables. Kinematic variables for each element are represented by three centroid velocities or displacements ($u_x^E$,$u_y^E$, $u_z^E$) and three rotation rates or rotations around centroid $G$ ($\Phi_x^E$,$\Phi_y^E$, $\Phi_z^E$).

To estimate inelastic deformations, it is necessary to evaluate the jump of velocities or displacements (for respectively limit and non-linear static analysis) on interfaces.

To do this, it is simply necessary to evaluate the displacement of a point P of the interface thought belonging alternatively to M and N, assuming that M and N are two wedge elements defining the interface. After trivial algebra, the jump can be evaluated in the global coordinates system as:

$$[\mathbf{U}(P)] = \mathbf{U}_M^G - \mathbf{U}_N^G + \mathbf{R}_M(P - G_M) - \mathbf{R}_N(P - G_N) \tag{1}$$

where $[\mathbf{U}(P)]$ is the displacement jump in $P$, $\mathbf{U}_I^G$ is the displacement vector of element $I$ centroid (point $G_I$) and $\mathbf{R}_I$ is a $3 \times 3$ rotation matrix for element $I$ containing rotations around centroid. Defined a local frame of reference $\mathbf{e}_1 - \mathbf{e}_2 - \mathbf{e}_3$ with $\mathbf{e}_3$ normal to the interface and $\mathbf{e}_1 - \mathbf{e}_2$ on the interface plane, denoting with $\mathbf{R_e}$ the rotation matrix with respect to the global coordinate system, jump of displacements (1) may be written in the local system as $[\tilde{\mathbf{U}}(P)] = \mathbf{R_e}[\mathbf{U}(P)]$ where tilde indicates quantities evaluated in the local system.

To solve the non-linear structural analysis problem, under some general hypotheses holding for materials exhibiting an elasto-plastic behavior, as for instance that the plasticity condition is piecewise-linearized with $r$ linearly elastic–plastic interacting planes in the space of superimposed stress and strain components, that the unloading of yielded stress-points does not occur and the continuum is discretized into Finite Elements, the incremental problem can be solved using the following quadratic programming formulation:

$$\begin{cases} \max \left\{ -\frac{1}{2}(\boldsymbol{\lambda}^E)^T \mathbf{H}^E \boldsymbol{\lambda}^E + (\boldsymbol{\lambda}^E)^T (\mathbf{N}^E)^T \mathbf{D}^E \boldsymbol{\varepsilon}^E \right. \\ \qquad \text{subject to} : \boldsymbol{\lambda}^E \geq \mathbf{0} \\ \qquad\quad \boldsymbol{\varepsilon}_t^E = \boldsymbol{\varepsilon}^E + \boldsymbol{\varepsilon}_{pl}^E \\ \qquad\quad \boldsymbol{\sigma}^E = \mathbf{D}^E \boldsymbol{\varepsilon}_{pl}^E \end{cases} \tag{2}$$

where $\mathbf{D}^E$ is the assembled elastic stiffness matrix, $\boldsymbol{\varepsilon}^E$ ($\boldsymbol{\varepsilon}_{pl}^E$) is the assembled elastic (plastic) part of the total strain vector $\boldsymbol{\varepsilon}_t^E$, $\mathbf{N}^E$ is the shape functions matrix of the used Finite Element, $\boldsymbol{\lambda}^E$ is the plastic multiplier vector, $\mathbf{H}^E$ is the hardening matrix and $\boldsymbol{\sigma}^E$ the assembled stress vector.

Within the FE model adopted, it can be shown that problem (2) may be re-written for the problem at hand (rigid elements with elastic–plastic interfaces) as follows:

$$\begin{cases} \min \left\{ \frac{1}{2} \left[ (\lambda^+ - \lambda^-)^T \mathbf{K}_{ep} (\lambda^+ - \lambda^-) + \mathbf{U}_{el}^T \mathbf{K}_{el} \mathbf{U}_{el} \right] - \mathbf{F}^T \mathbf{U}_{el} \right. \\ \qquad \text{subject to} : \boldsymbol{\lambda}^+ \geqslant \mathbf{0}\ \boldsymbol{\lambda}^- \geqslant \mathbf{0} \end{cases} \tag{3}$$

Assuming that the structural model has $n_{in}$ interfaces and $n_{el}$ elements, symbols in Eq. (3) have the following meaning:

1. $1\ \mathbf{K}_{el}$ is a $6n_{el} \times 6n_{el}$ assembled matrix, collecting elastic stiffness of each interface.
2. $\lambda^+$ and $\lambda^-$ are two $10n_{in}$ vectors of plastic multipliers, collecting plastic multipliers of each non-linear spring (e.g. flexion, shear, etc.).
3. $\mathbf{K}_{ep}$ is a $10n_{in} \times 10n_{in}$ assembled matrix built from diagonal matrices of hardening moduli of the interfaces.
4. $\mathbf{U}_{el}$ is a $6n_{el}$ vector collecting the displacements and rotations of the elements.
5. $\mathbf{F}$ is a $6n_{el}$ vector of external loads (forces and moments) applied on element centroids.

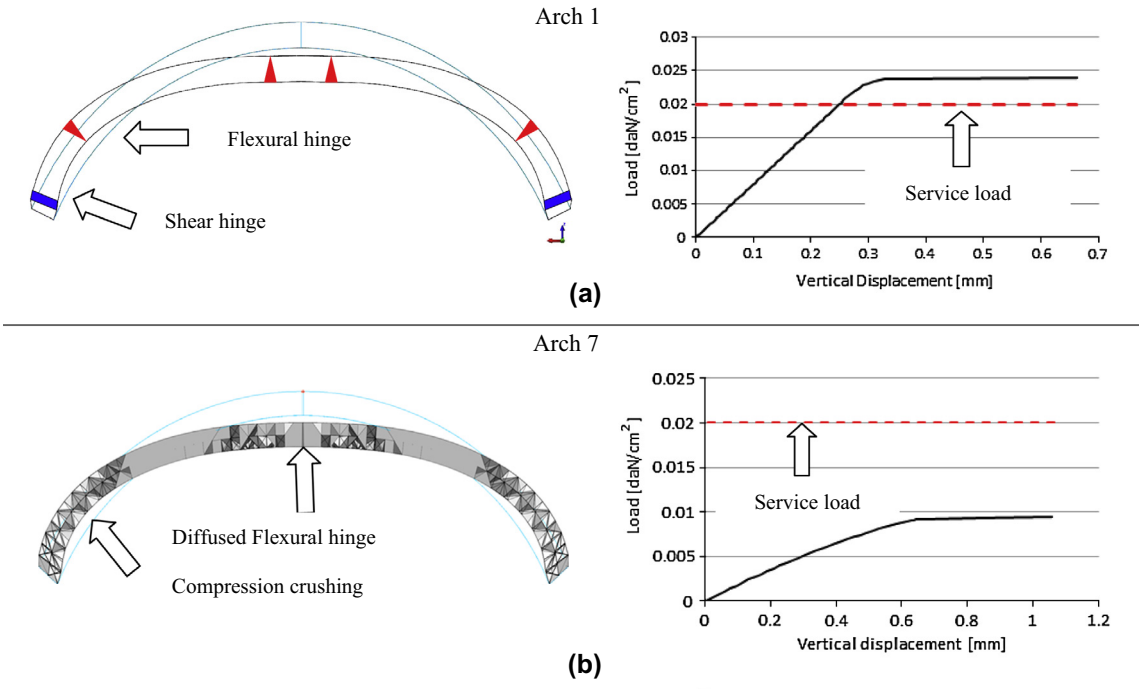


**Fig. 12.** Results from the second simplified approach (non-straight arches). (a) Arch 1. Left: deformed shape at failure and position of the plastic hinges at collapse. Right: load–displacement curves compared with the service load present. (b) Arch 7. Left: deformed shape at failure and damage map distribution. Right: load–displacement curves compared with the service load present.

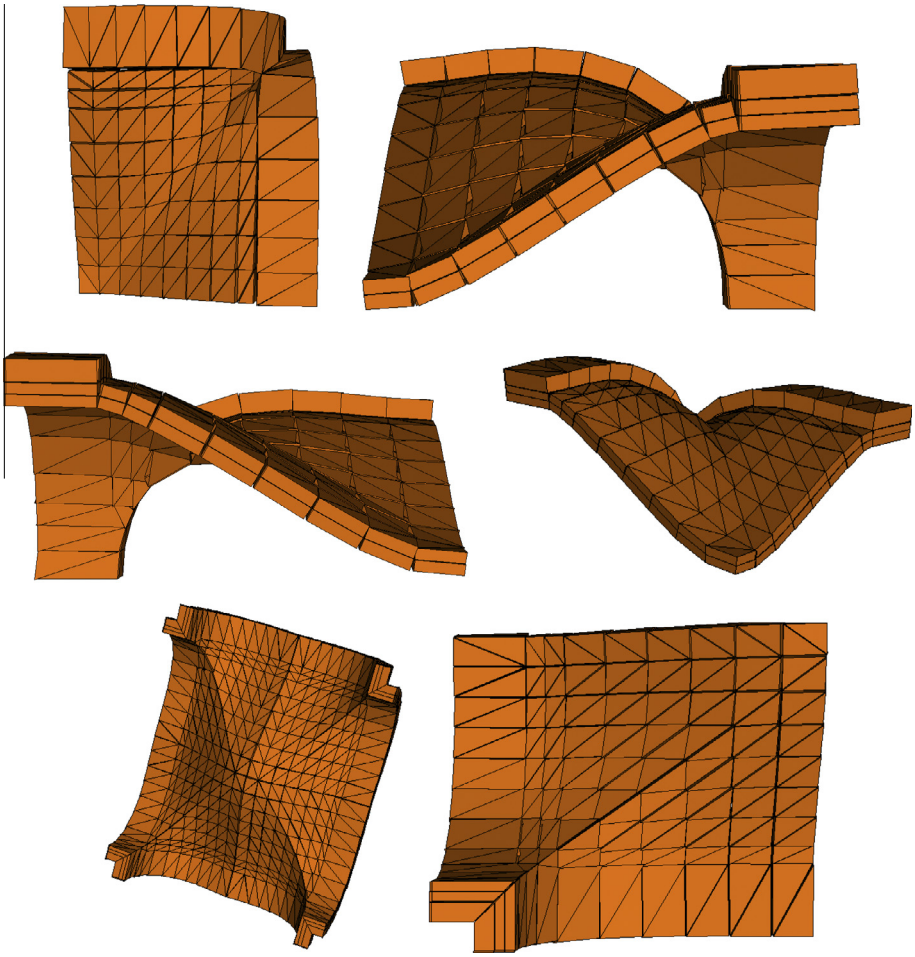

**Fig. 13.** Arch without infill, BC1. Limit analysis and incremental software deformed shapes at collapse.

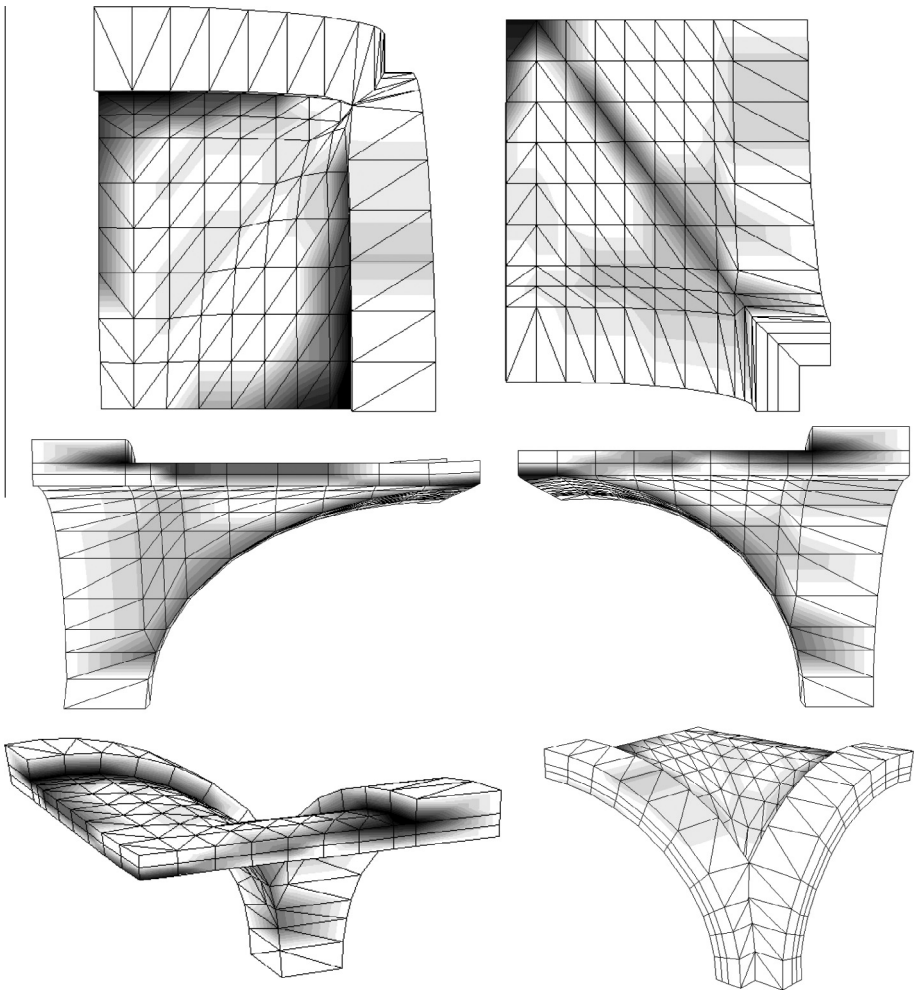

**Fig. 14.** Arch without infill, BC1. Normalized plastic dissipation patch.

Typically, the independent variable vector is represented by element displacements $\mathbf{U}_{el}$ and plastic multiplier vectors $\boldsymbol{\lambda}^{+}$ and $\boldsymbol{\lambda}^{-}$.

At a structural level, within the non-linear code used, the quadratic programming procedure adopted, see [28–30], requires an approximation of the stress–strain curves by means of linear piecewise constant functions, to deal with elastic perfectly plastic materials on a sub-increment step and hence solve problem (3) in incremental form.

Curves to approximate are obtained using a well established elasto-plastic model, already utilized in [29], where the reader is referred to for further details.

In the model, mortar is supposed obeying a Mohr–Coulomb failure criterion with tension cutoff and linearized cap in compression (shape of the linearized compressive cap is denoted with symbol $\Psi$). In the non-linear model, the post-elastic behavior exhibits softening, ruled by distinct fracture energies, $G_{\mathrm{I}}$ and $G_{\mathrm{II}}$, in tension and shear. Compressive behavior is ruled by several stress values and strain parameters, to reproduce consistently crushing. They are stress $f_{ce}$ at the elastic limit, peak compressive strength $f_{cp}$ corresponding to a plastic strain parameter equal to $\varepsilon_p$, stress $f_{cm}$ at crushing corresponding to a plastic strain parameter equal to $\kappa_m$ and residual stress $f_{cr}$. Full details of the model can be found in [29,30], where the reader is also referred to for a detailed description of the inelastic model in compression.

Mechanical properties adopted to simulate the behavior of the masonry vaults under consideration are summarized in Table 1.

The resultant stress–strain behaviors in compression and tension and under shear with different levels of vertical pre-compression of the masonry material of Table 1 are represented in Fig. 4, with the corresponding stepped function used at a structural level to simulate the non-linear behavior of the vault.

When the limit analysis software is used, the material considered is rigid-plastic with associated flow rule, and only strength values reported in Table 1 are utilized. In particular, a Mohr–Coulomb failure criterion with tension cutoff and linearized cap in compression, fully defined by tensile strength $f_{\mathrm{t}}$, cohesion $c$, friction angle $\Phi$, compressive strength $f_{\mathrm{cp}}$ and shape of the linearized compressive cap (identified by the angle $\Psi$) are considered. To obtain collapse loads and failure mechanisms for the structure at hand, the discretized FE limit analysis problem is mathematically translated into standard linear programming. In the framework of the upper bound theorem of limit analysis, the objective function to minimize is represented by the total internal power dissipated minus the power expended by the loads independent from the collapse multiplier. Equality constraints are represented by associated plasticity flow rules, boundary conditions and normalization of the external power expended by the load multiplier, this latter condition allowing to univocally identify the failure mechanism (in limit analysis, indeed, only the shape of the failure mechanism may be determined). Inequality constraints translate into mathematics the physical requirement that plastic multipliers are non-negative. Within the FE discretization by means of rigid elements, independent variables

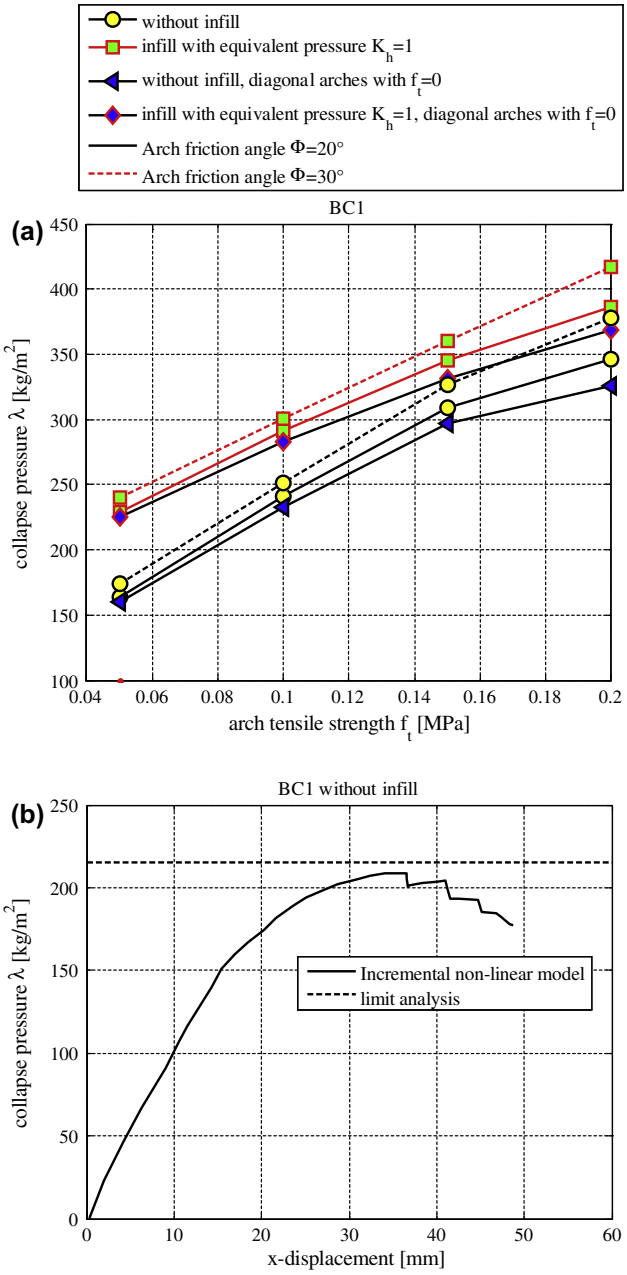


**Fig. 15.** Arch without infill, BC1. (a) Live loads corresponding to the collapse of the vault at different values of mortar tensile strength and friction angle. (b) Pressure-vertical displacement curves obtained with the non-linear code.

are represented by element centroid velocities, rotation rates around centroid and plastic multipliers at the interface between adjoining elements.

As already pointed out, Table 1, elastic moduli and values of compressive and tensile strength are taken in general agreement with the Italian code [38,39]. For other quantities at failure or describing the post-peak behavior, there aren't specific indications available. In particular, the evaluation of the relation between cohesion and tensile strength is still an open research issue, depending on several concurring factors, as mortar quality and masonry texture. Similar considerations hold for the shape of the cap in compression. For this reason, reference is made to existing literature in this field [43–46]. The same procedure is followed for the choice of Mode I and Mode II fracture energies and for the evaluation of

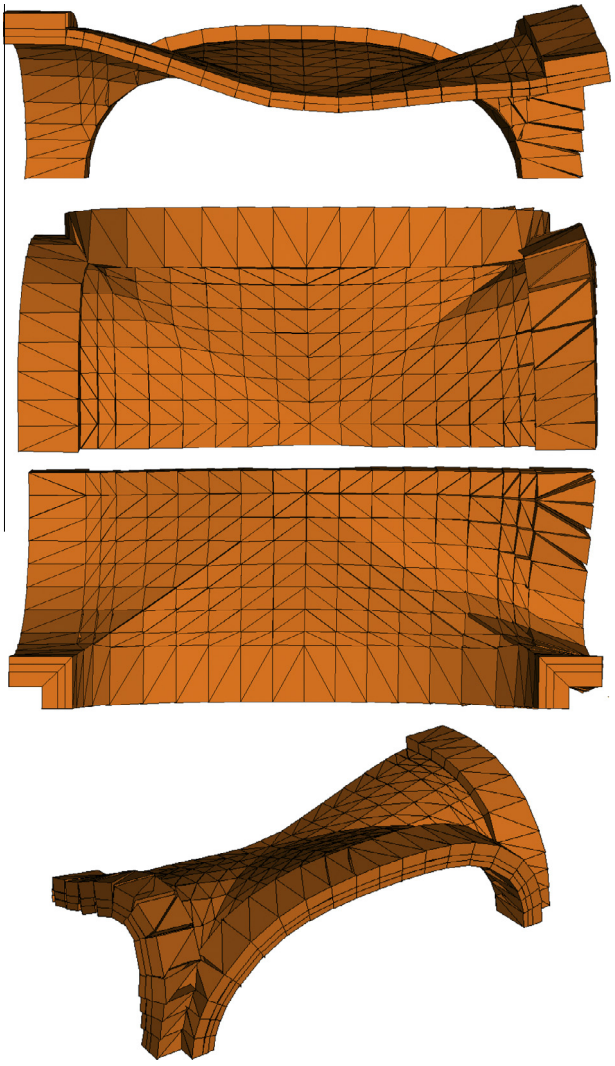

**Fig. 16.** Arch without infill, BC2. Limit analysis and incremental software deformed shapes at collapse.

the softening behavior in compression [28,29,45]. Friction angle adopted is again in general agreement with NTC 2008 [38].

## 4. Numerical simulations

Several numerical simulations are conducted with the aforementioned approaches, varying (1) boundary conditions, (2) infill modeling, (3) materials mechanical properties and (4) presence of FRP strips as reinforcement.

- Boundary conditions

The application of realistic boundary conditions to a single vault extracted from the context is not an easy task and is crucial for a deep understanding of the structural behavior under increasing vertical loads. As a matter of fact, the high number of vaults to deal with (108), makes impossible a detailed analysis of each specific case extracted from the context, with the application of ad-hoc boundary conditions present case by case in reality. To conflict with such a need, it is worth noting that sometimes boundary conditions are very different and quite specific; indeed, some of the vaults rest on load-bearing walls, some others on columns, in other

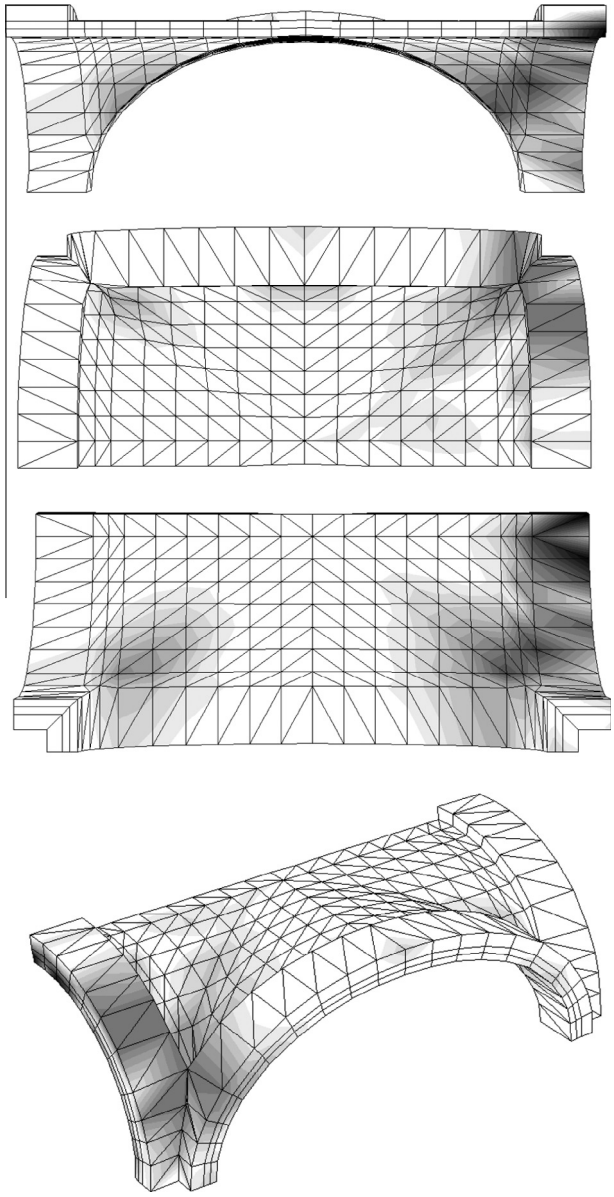

**Fig. 17.** Arch without infill, BC2. Normalized plastic dissipation patch.

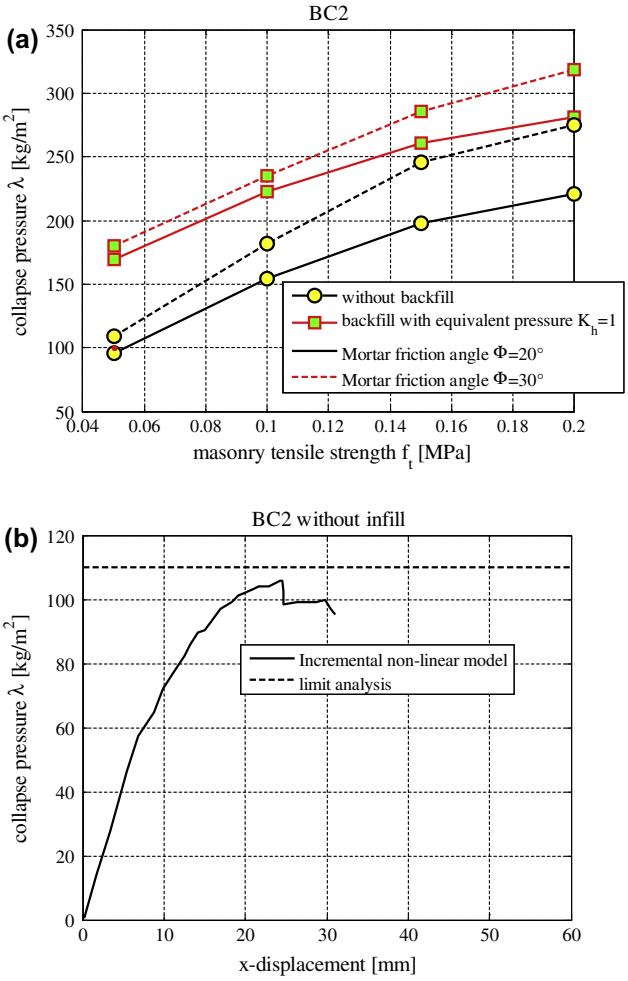


**Fig. 18.** Arch without infill, BC2. (a) Live loads corresponding to the collapse of the vault at different values of mortar tensile strength and friction angle. (b) Pressure-vertical displacement curves obtained with the non-linear code.

cases columns are strengthened with tie-rods, disposed either on single or both directions. As a consequence, it appears clear that each cross vault would require the study of ad hoc boundary and load conditions, specific for each relevant case. Considering that the effort needed in this case would be prohibitive, the alternative strategy used here – also followed when traditional methods of decomposition into arches are adopted – is the application of "idealized" boundary conditions, representative of the "average" situation encountered in practice. Such choice is more methodological than practical and is focused at analyzing a single vault extracted from the context (i.e. without considering the thrust forces of the vaults and arches on the eventually present supporting pillars and walls). The final aim is to put at disposal a set of information that may be considered "general", to promote a unique strengthening intervention scheme that, independently from specificities, is applicable in any case.

In this context, two boundary conditions are studied in detail, hereafter labeled as BC1 and BC2, realistically reproducing what occurs in practice on average. The former boundary condition system, BC1, simulates well the behavior of a central vault under increasing vertical loads, whereas the latter, BC2, reproduced what occurs for a lateral vault.

In particular, for the first configuration (central vault), all buttresses and the boundary arches are constrained not to translate in the horizontal direction perpendicular to the edge, whereas for the second configuration (external vault) the elements belonging to one edge (i.e. one boundary arch and two buttresses) are allowed to move also perpendicularly to the edge, as shown schematically in Fig. 1.

When dealing with the simplified approach, the distinction between the two boundary conditions may not be done.

- Loads

Before any consideration involving horizontal actions, a safety assessment of the structures under vertical loads is required. Loads considered in the analyses are masonry (18 kN/m$^3$), infill (18 kN/m$^3$), and floors self weight (3.4 kN/m$^2$). A further arbitrary distributed load equal to 0.4 kN/m$^2$ is also applied, in agreement with Italian code, in order to take into account the incidence of non-carrying separation walls at the first floor. Within the limit analysis approach it is interesting to evaluate what is the

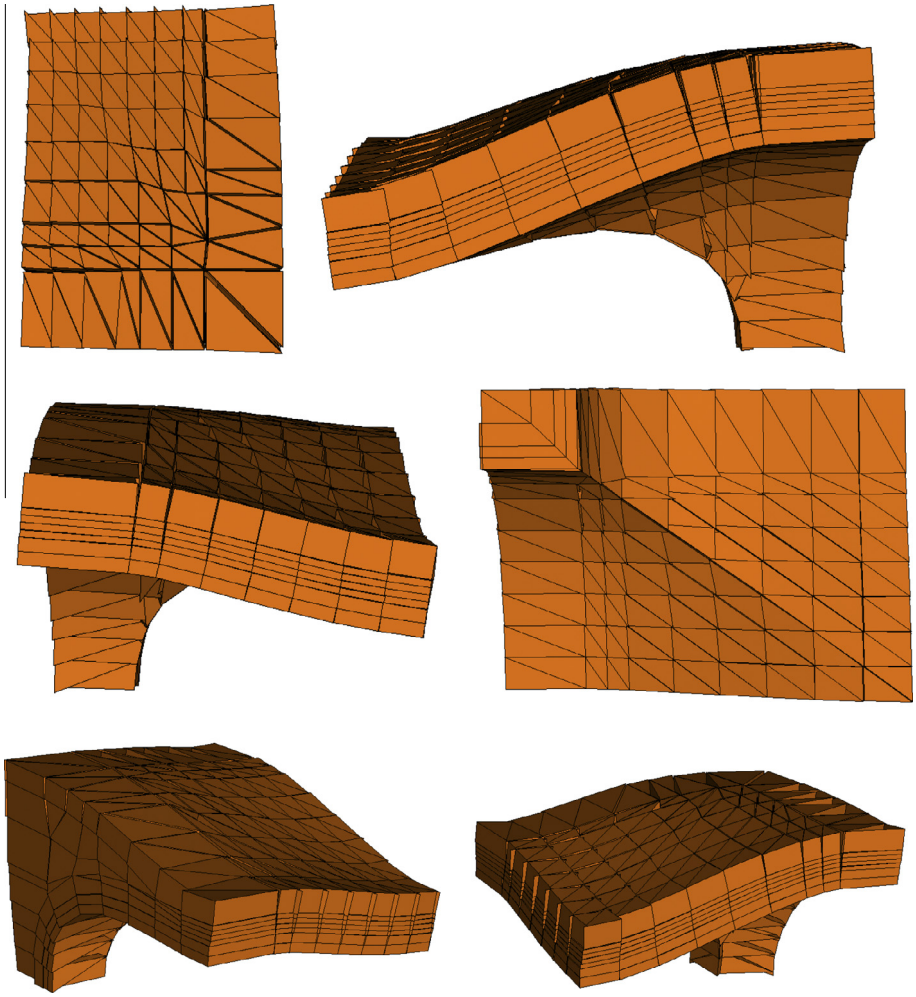

**Fig. 19.** Arch with infill, BC1. Limit analysis and incremental software deformed shapes at collapse.

maximum distributed live load that can be carried by the structure up to collapse. On the contrary, thrust lines are evaluated with a variable load (C1 category for the Italian code) equal to 3 kN/m$^2$.

- Infill effect

The role played by the infill is accounted for both in an approximate (i.e. adding a stabilizing horizontal pressure following an earth pressure model) or rigorous way modeling backfill by means of wedge elements obeying a Mohr–Coulomb failure criterion, characterized by moderately high friction angle and very low cohesion. However, it should be noted that the completion of infill in the vaults of buildings were generally built with less care than in the case of masonry bridges and therefore the mechanical parameters could be worse and more uncertain.

However, the infill, as clearly shown by Fig. 5 and as observed by the authors with a direct in-situ inspection, is mainly composed of pebbles, fragments of brick and other rubbles. Sometimes a huge amount of lime is also present. It appears therefore rather suitable to model it assuming the same mechanical properties of a cohesion-less material.

In both cases, the increase of the load bearing capacity obtained by means of the installation of extrados FRP strips, as recommended within the planned restoration intervention, is numerically estimated.

- Vault mechanical properties

A comprehensive numerical sensitivity analysis is conducted varying in a wide range mortar joints tensile strength and friction angle. Values recommended by the Italian Code are progressively decreased and increased up to 4 times their original value for the cohesion and 1.5 times for the friction angle.

Mechanical properties of mortar and brick are assumed as in Table 1 and the corresponding homogenized behavior is summarized in Fig. 4.

- Effect of the reinforcement

Two different strategies of reinforcement, at the extrados (labeled with the symbol ER) or at the intrados (IR) with innovative materials are planned, depending if the first floor is accessible or not. When the first floor is accessible, extrados reinforcement as in Fig. 6 is adopted. In case the first floor is not accessible, an intrados strengthening with GFRP grids is proposed. The first intervention is aimed at precluding the formation of extrados hinges and close Sabouret's cracks; nonetheless, its efficacy appears may vanish in case the backfill is fully restored. As a matter of fact, the installation of the strips requires removing completely the backfill, which has to be re-positioned after the strengthening intervention with the same mechanical properties.

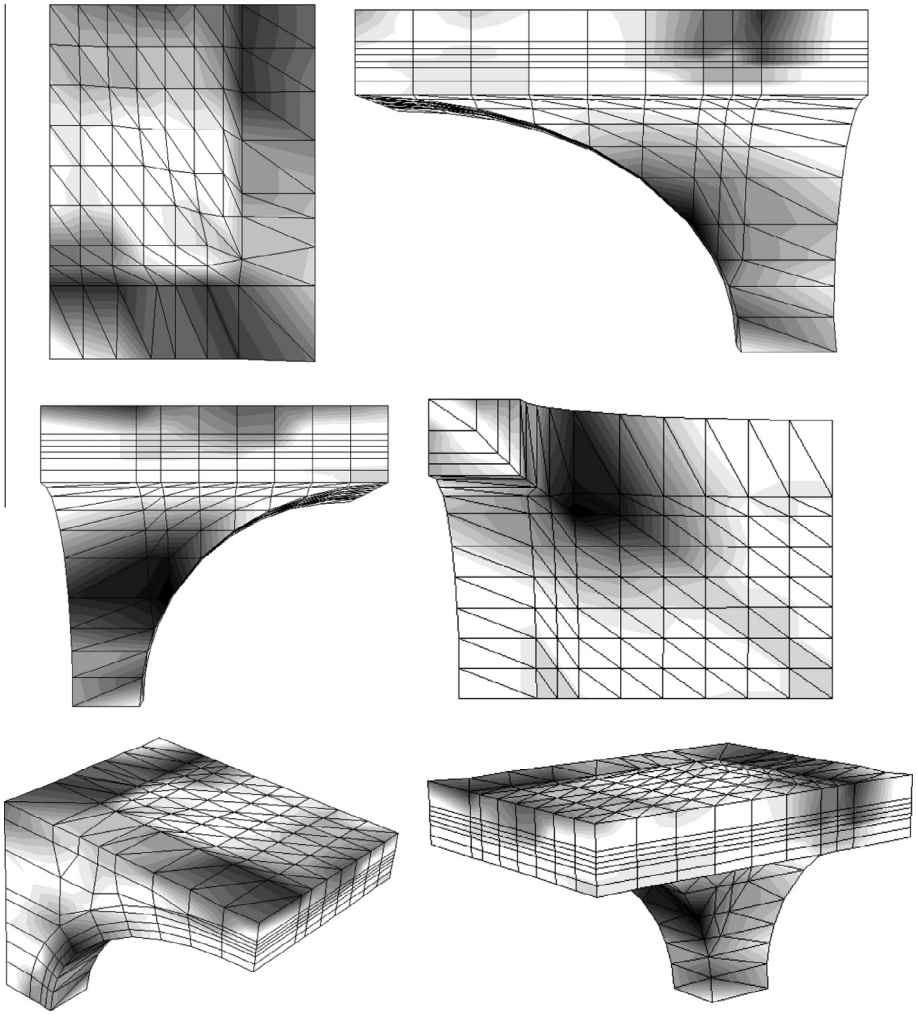

**Fig. 20.** Arch with infill, BC1. Normalized plastic dissipation patch.

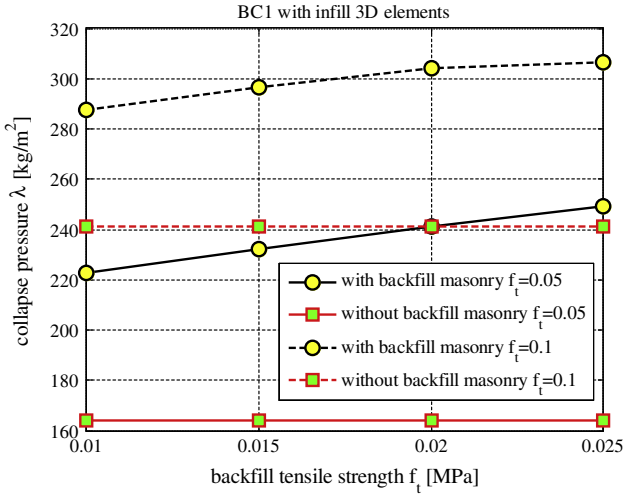


**Fig. 21.** Arch with infill, BC1. Live loads corresponding to the collapse of the vault at different values of infill tensile strength and arch tensile strength equal to 0.05 and 0.1 MPa.

When this last hypothesis does not hold and a perturbation into infill strength is introduced, a decrease (or generally a variation) of the beneficial role played by the infill may result. In addition, the disposition of the diagonal reinforcement appears rather inefficient against the propagation of intrados cracks, which appears one of major causes of degradation of the structures under consideration.

## 5. Results and discussion

In the present Section, the results of the comparative analysis performed with the traditional decomposition method [2], first and second approach, the full 3D homogenized limit and non-linear code are reported and discussed in detail.

The results of the analyses conducted by means of the simplified decomposition (first approach, straight arches and thrust lines) are reported from Figs. 8–11.

As can be noted from Fig. 8, the shorter perimeter arch (hereafter labeled as arch A) is substantially safe under vertical loads, being the thrust line all internal to the transversal section (no tension material hypothesis). When dealing with the larger perimeter arch (labeled as arch B), having an elliptic shape, the thrust line still remains within the thickness of the wall, but very near to the extrados in correspondence of the buttresses. Under a no tension material model assumption, while the safety of the arch is not compromised, it is expected the formation of a hinge in this position, with cracks formation.

For internal arches, it is found that both small arches A and B are safe, Fig. 9, whereas for the intermediate arches, Fig. 10, the

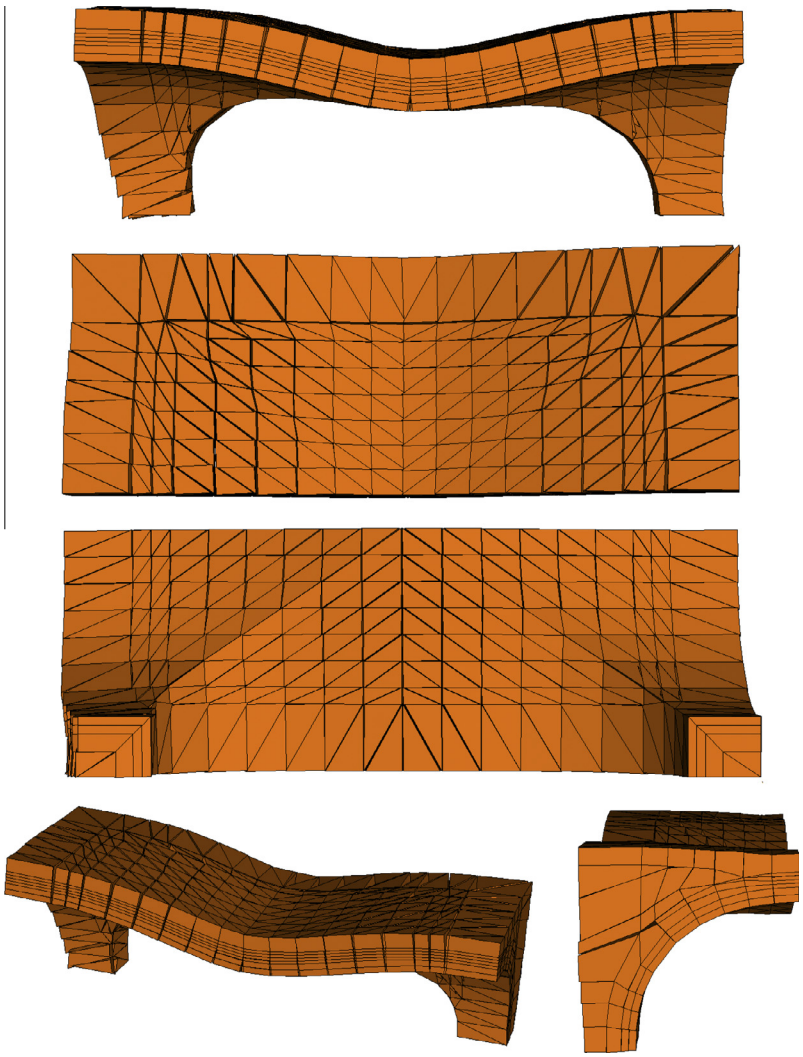

**Fig. 22.** Arch with infill, BC2. Limit analysis and incremental software deformed shapes at collapse.

thrust lines exit for the arch thickness in several points, both for A and B configurations. A kinematic limit analysis is conducted in these cases with a Matlab implementation of a code dealing with 1DOF structures, with results similar to those obtained with the program Ring [40], also considering the stabilizing effect by means of a linear horizontal confining pressure, as indicated in Fig. 10. The formula utilized for the evaluation of the passive pressure of the infill is $\sigma_p = \sigma'_v K_p$, where $K_p = (1 + sin\varphi)/(1 + sin\varphi)$ and $\varphi$ indicates the infill internal friction angle, assumed according to specialized literature in this field equal to 30°.

By means of the kinematic analysis, the value of the collapse multiplier associated to the vertical distributed loads (floor weight and live load) is $\lambda = 0.33$, with formation of a plastic hinge at 33°.

Considering the stabilizing contribution of the infill (horizontal pressure), the collapse multiplier is extremely high ($\lambda = 8.7$) and the plastic hinge slightly changes its position (35°).

Arches along the diagonals are analyzed in Fig. 11, assuming a distribution of concentrated vertical and horizontal loads determined knowing the reactions found previously for the internal and external arches.

Observing the corresponding thrust line, found assuming for the diagonal arches, which are without ribs, a linear elastic material. It can be deduced that they are unsafe in several regions (base, middle eight, top), thus implicitly justifying the formation of the diagonal cracks observed in reality.

The results obtained with the second simplified approach (non-straight arches) are reported in Fig. 12. To obtain the results shown in Fig. 12, a damage plasticity model embedded into the commercial code DIANA v7.3 was used, being not possible an analysis of the arches with variable thickness within the approach utilized for straight arches. A very low tensile strength (0.05 MPa) obeying a Drucker–Prager failure criterion (friction angle equal to 30°) and compression peak strength equal to 2.4 MPa were assumed. Only results obtained for Arch 1 and Arch 7 (Fig. 7-b) are reported for the sake of conciseness: authors experienced, indeed, that the remaining arches exhibited an intermediate behavior.

As can be noted from Fig. 12-a, where the deformed shape at collapse with a graphical indication of formed plastic hinges and load displacement curve are represented, Arch 1 is safe under the design live load acting. In addition, it can be observed that failure is due to a rather clear formation of flexural plastic hinges (red symbols) at the crown and in an intermediate position. Rather evident shear sliding (blue symbols) is also present in correspondence of the abutments.

When dealing with Arch 7 (results are summarized in Fig. 12-b), the load carrying capacity is largely insufficient when compared

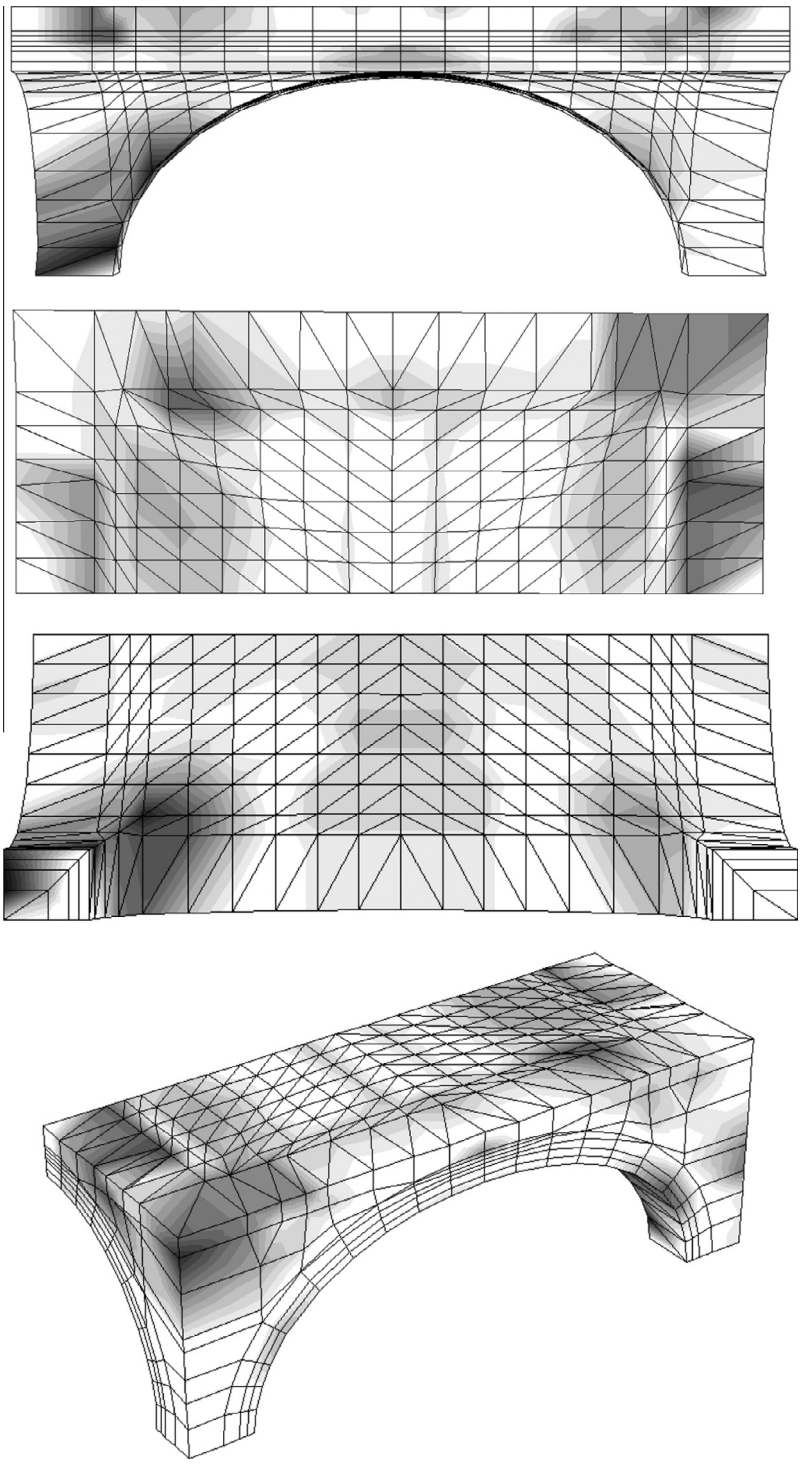

**Fig. 23.** Arch with infill, BC2. Normalized plastic dissipation patch.

with the acting live load. In addition, failure of the arch occurs for a diffused crushing in correspondence of the abutments and plastic hinges at the crown spreading laterally, with a clear diffusion of the tensile cracks.

From a detailed analysis of results summarized in Fig. 12, again it can be affirmed that even the second approach (analogously to what occurs for the first simplified procedure) does not appear fully reliable, providing largely unsafe results (Arch 7) under acting service loads.

The results of the analyses conducted with the full 3D FE models are reported from Figs. 13–18, assuming not to discretize the infill with six-noded wedge elements and different materials. The mesh used for the numerical simulations is depicted in Fig. 1.

In particular, from Figs. 13–15 the results obtained with the first boundary condition hypothesis (BC1) are summarized, whereas from Figs. 16–18 the same results are replicated for the second boundary condition (BC2). In both cases, infill is not modeled.

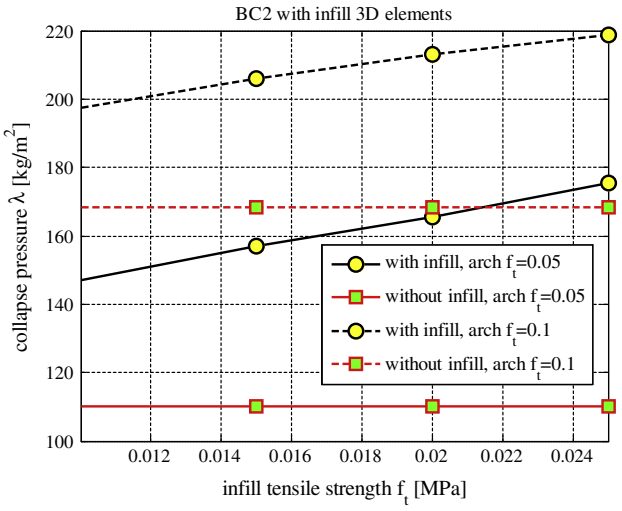


**Fig. 24.** Arch with infill, BC2. Live loads corresponding to the collapse of the vault at different values of infill tensile strength and arch tensile strength equal to 0.05 and 0.1 MPa.

As it is possible to notice from both deformed shapes at collapse and power dissipation patch (Figs. 13 and 14 for BC1 and Figs. 16 and 17 for BC2), the full detachment of the perimeter arches is observed in both cases, with a quite clear shear collapse of one of the external short arches in case of BC2, due to the possible out-of-plane movement allowed for the particular boundary condition imposed.

Thanks to the very limited computational cost required by both limit analysis and non-linear incremental code, mechanical properties of the masonry are varied in a wide range. In particular, four different values for the tensile strength (0.05, 0.10, 0.15 and 0.20 MPa) and two values of the friction angle (20°, 30°) are assumed in the simulations.

Values of cohesion are assumed always equal to $1.2f_t$ and hence, in the simulations, they take values equal to 0.06, 0.12, 0.18 and 0.24 MPa respectively. Compression strength is always kept equal to 2.4 MPa.

It is worth noting here that, for regular masonry with clay bricks and mortar with weak mechanical properties, with a level of knowledge LC1 and confidence factor Fc = 1.35, Italian code NTC 2008 [38] imposes to assume a cohesion for masonry equal to 0.06 MPa and a compressive strength equal to 2.4 MPa (lower bound values of the interval).

In both the limit analysis and the non-linear incremental model, for both boundary conditions, it is possible to take into account the stabilizing role played by the infill adding in the model a horizontal pressure, dependent on the load multiplier (more precisely on dead and live loads). Safely, it is assumed arbitrarily that the infill applies to the structure a horizontal pressure with coefficient $K_h$ kept equal to 1.

Collapse loads found with both procedures under BC1 and BC2 hypotheses are depicted in Figs. 15 and 18 respectively. It is worth noting that the maximum live load which can be applied to the structure without the activation of a failure mechanism is quite low. This is especially true for BC2, where one boundary arch can fail with out-of-plane movements.

It is interesting to notice that, in Fig. 15, the results of two sets of simulations assuming diagonal arches with zero tensile strength are represented. For the sake of conciseness, only the case with friction angle equal to 20° is investigated. The hypothesis of zero strength in tension for diagonal arches appears quite realistic, since the vault is not ribbed and there is a clearly visible interlocking deficiency where perpendicular bricks meet, Fig. 3. In Fig. 3, indeed, it is possible to notice that the interconnection between vault quadrants is exclusively secured by mortar (sometimes not anymore present due to degradation phenomena). Results of the simulations assuming a no-tension material for diagonal arches agree rather well with intuition. As shown by Fig. 15, collapse pressures obtained assuming that diagonal arches behave as a no-tension material are slightly lower than those evaluated with finite strength. The difference is negligible for small masonry tensile strengths (i.e. when a reasonable approximation of a no-tension material is assumed for masonry), but becomes more relevant for increased values of $f_t$, with a percentage difference

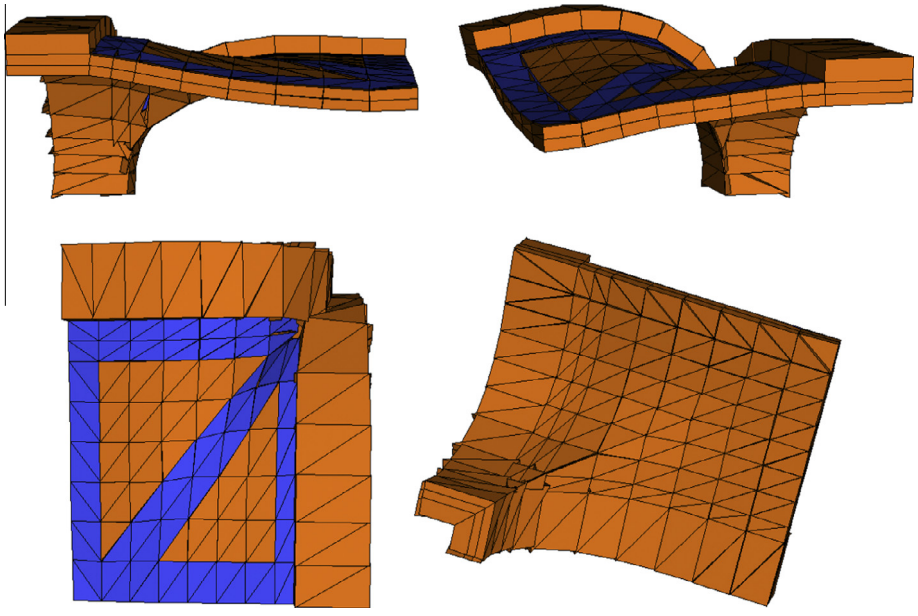

**Fig. 25.** Extrados reinforcement, arch without infill, BC1. Limit analysis and incremental software deformed shapes at collapse.

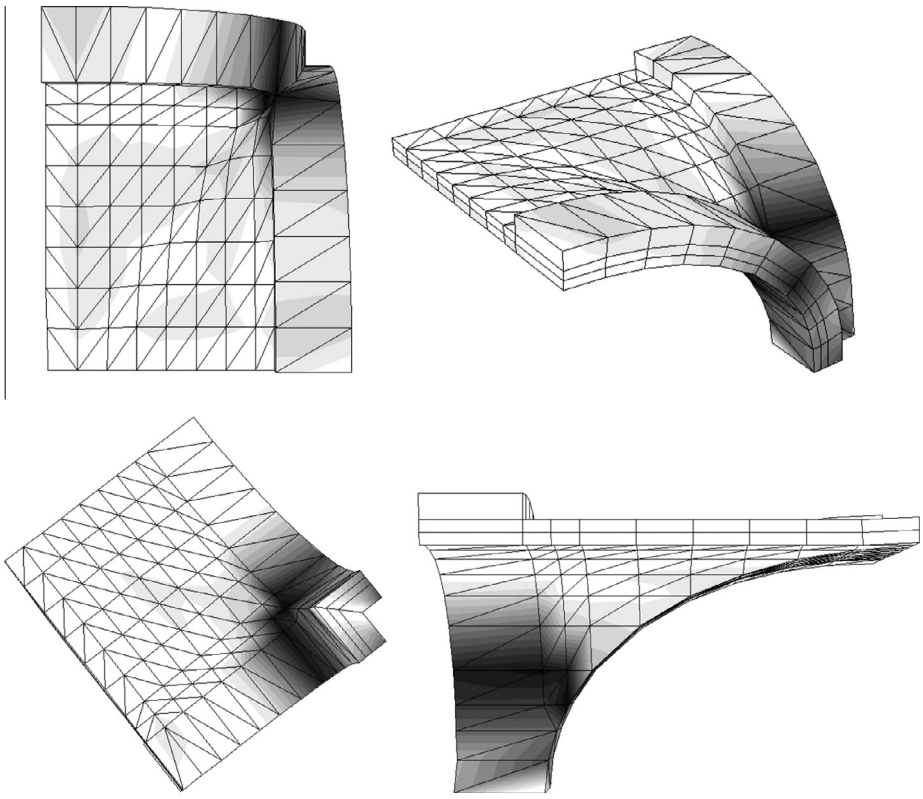

**Fig. 26.** Extrados reinforcement, arch without infill, BC1. Normalized plastic dissipation patch.

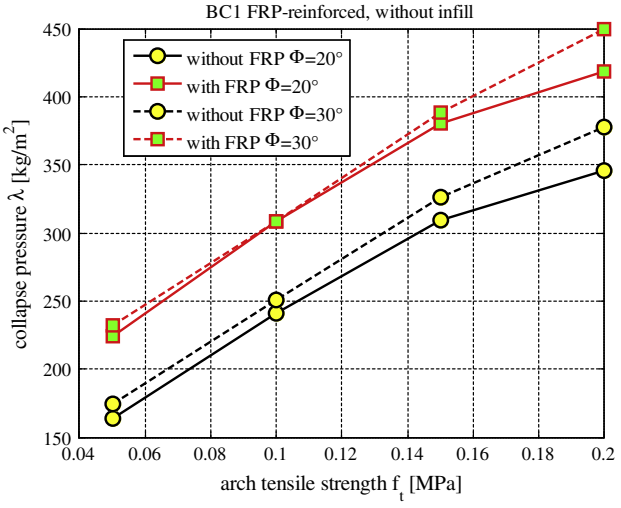


**Fig. 27.** Extrados reinforcement, arch without infill, BC1. Live loads corresponding to the collapse of the vault at different values of mortar tensile strength and friction angle.

on the estimated collapse pressure of around 5% for $f_t$ equal to 0.2 MPa. Similar results, not reported for the sake of conciseness, are obtained for BC2 case.

From simulations results, the following considerations may be drawn: (1) as expected BC2 is less safe than BC1, (2) the stabilizing role played by the backfill results into an increase of the collapse live pressure of about 70 kg/m$^2$ for very low tensile strength of the arches and of about 30–40 kg/m$^2$ for more resistant masonry (3) the vault loaded with a live load equal to 300 kg/m$^2$ is near its collapse state and may require a strengthening intervention.

When dealing with the discretization of the backfill into Finite Elements, which definitely is the most appropriate modeling strategy to adopt, the mesh depicted in Fig. 1 is utilized.

Within the sensitivity analyses carried on, mechanical properties of the backfill are assumed obeying a Mohr Coulomb failure criterion with very low cohesion (from 0.010 to 0.025 MPa) and a moderately high friction angle equal to 37°. Results of the numerical analysis for BC1 are summarized in Figs. 19–21 and for BC2 in Figs. 22–24 respectively. Deformed shapes show a quite different behavior of the vault when compared to the simulations without backfill. Again Sabouret's cracks are visible in both BC's cases but here a flexural deformation of the vault in its central part is experienced, with clearly visible openings along diagonal arches, not present in the model without backfill. Plastic dissipation patches represented in Fig. 20 (BC1) and Fig. 23 (BC2) confirm the formation of cracks along diagonals and at the interface between ribbed perpendicular arches and vault.

The deformed shapes obtained increasing mortar tensile strength are qualitatively similar to those reported in Fig. 19 (BC1) and Fig. 22 (BC2), which correspond to the lower tensile strength investigated (0.05 MPa) and a friction angle equal to 20°.

The introduction of FRP strips at the extrados proved to increase the collapse loads in both configurations. The results of the simulations are summarized from Figs. 25–27 for BC1 configuration (following the order of the figures, respectively the deformed shape at collapse, power dissipation patch and collapse load are depicted) and from Figs. 28–30 for BC2.

In particular, analyzing the collapse loads of the structure in presence and absence of reinforcement at different values of masonry tensile strength, as shown by the diagrams in Fig. 27 (BC1) and Fig. 30 (BC2), it is possible to notice a quite regular increase of the load bearing capacity of the structure (increase up

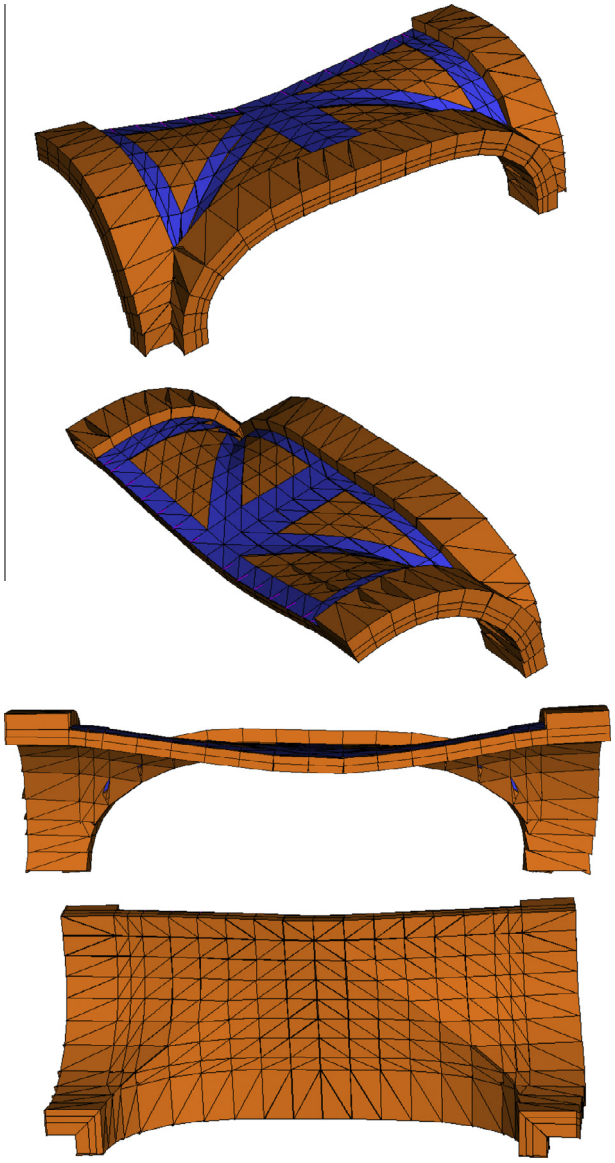

**Fig. 28.** Extrados reinforcement, arch without infill, BC2. Limit analysis and incremental software deformed shapes at collapse.

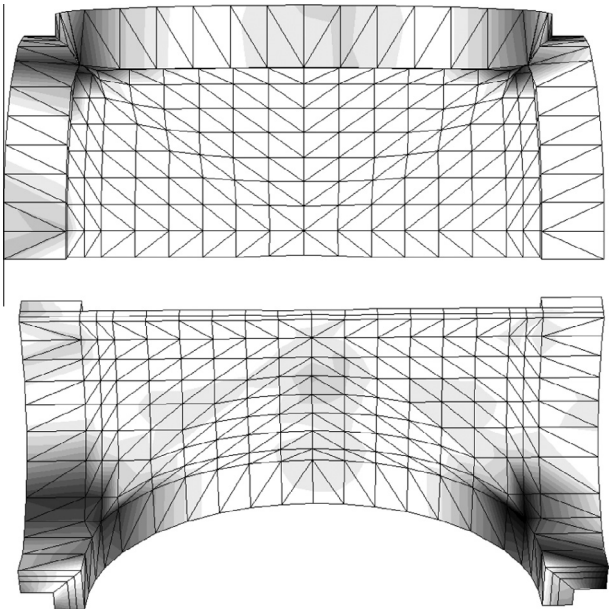

**Fig. 29.** Extrados reinforcement, arch without infill, BC2. Normalized plastic dissipation patch.

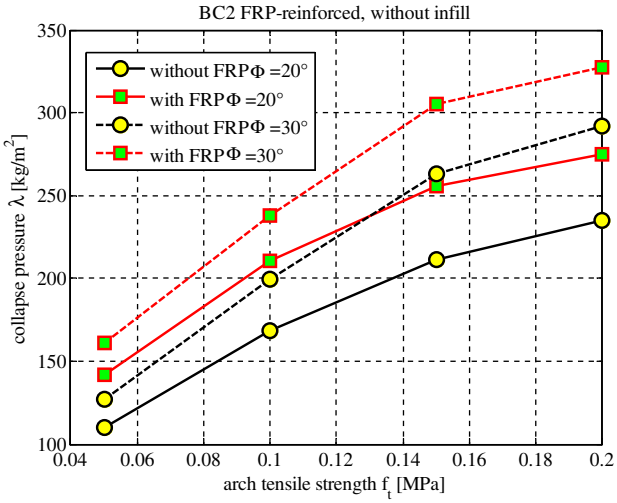


**Fig. 30.** Extrados reinforcement, arch without infill, BC2. Live loads corresponding to the collapse of the vault at different values of mortar tensile strength and friction angle.

to almost 30% for very low tensile strength and to around 15% for masonry with good mechanical properties), which however remains insufficient for BC2 with masonry having low tensile strength (collapse pressure < 200 kg/m$^2$). The failure mechanism remains substantially unchanged with respect to the unreinforced case, exception made for a slight closure of the diagonal cracks, where delamination of the strip occurs.

In the models analyzed with reinforcement, the infill is not taken into account (only the corresponding gravity load is modeled as distributed vertical pressure) in order to consider the most critical situation for the structure and also to partially take into account that the removal of the infill and its subsequent re-placement could visibly alter the stabilizing role of the infill.

It is worth noting, indeed, that the major drawback of installing strips at the extrados is the removal of the infill and its subsequence reallocation over the installed strengthening. This could considerably alter the beneficial capacity of the infill to carry and distribute external loads, making the numerical evaluation of the maximum collapse load quite questionable.

## 6. Conclusions

An existing masonry cross vault typology showing dangerous deterioration and diffused crack patterns has been analyzed numerically with different advanced procedures, including non-linear FEs and limit analysis. A 3D discretization by means of rigid infinitely resistant wedges where all the non-linearity is concentrated on interfaces between adjoining elements has been used. Two different boundary conditions and the presence of the infill have been taken into account, performing analyses at different values of masonry strength, eventually modeling the infill behaving as a frictional material with very small cohesion.

From simulations results, it has been found that the approach commonly used in practice to study cross vaults by means of the assemblage of single arches is not always reliable, providing failure loads and mechanisms sometimes different from the real ones.

Some discrepancies are found also with the decomposition into non straight arches, an alternative simplified procedure particularly suited for gothic vaults. Similarly to what occurs for masonry arch bridges, simulations address that the role played by the infill is rather important, providing a useful stabilizing effect. Nevertheless, the completion of the infill in the vaults was generally done, in the past, with less care than that used for bridges. Therefore, it is reasonable to say that the mechanical parameters adopted could be overestimated and more uncertainties are present in the determination of the collapse loads.

A final set of simulations is performed reinforcing the vaults at the extrados with FRP strips, as suggested in the real rehabilitation intervention, Fig. 6. Whilst it is found numerically that FRP has a relevant role in increasing the load bearing capacity, some doubts arise in the practical execution of the intervention, which requires the total removal of the infill and its subsequence reallocation, with effects hardily predictable.

## References


[1] Benvenuto E. An introduction to the history of structural mechanics. Volume II. Vaulted structures and elastic systems. Berlin-New-York: Springer-Verlag; 1991.
[2] Como M. Statics of historic masonry constructions. Berlin: Springer-Verlag; 2013.
[3] Paradiso M, Tempesta G, Galassi S. X-Vaults: a software for the analysis of the stability of masonry cross-vaults. IJCSI 2012;9(2). March 2012, ISSN (Online) 1694-0814.
[4] Mark R, Abel JF, O'Neill K. Photoelastic and finite-element analysis of a quadripartite vault. Exp Mech XIII 1973:322–9.
[5] Heyman J. The safety of masonry arches. Int J Mech Sci 1969;43:209–24.
[6] Heyman J. Equilibrium of shell structures. Oxford: Oxford University Press; 1977.
[7] Heyman J. The masonry arch. J. Wiley & Sons; 1982.
[8] Huerta S. Mechanics of masonry vaults: the equilibrium approach. In: Lourenço PB, Roca P, editors. Proc. Historical Constructions, Guimarães PT; 2001.
[9] Brencich A, Morbiducci R. Masonry arches: historical rules and modern mechanics. Int J Archit Heritage 2007;1(2):165–89.
[10] Lucchesi M, Padovani C, Pasquinelli G, Zani N. On the collapse of masonry arches. Meccanica 1997;32:327–46.
[11] Lucchesi M, Padovani C, Pasquinelli G, Zani N. The maximum modulus eccentricity surface for masonry vaults and limit analysis. Math Mech Solids 1999;4:71–87.
[12] Audenaert A, Fanning P, Sobczak L, Peremans H. 2-D analysis of arch bridges using an elasto-plastic material model. Eng Struct 2008;30:845–55.
[13] Drosopoulos GA, Stavroulakis GE, Massalas CV. Limit analysis of a single span masonry bridge with unilateral frictional contact interfaces. Eng Struct 2006;28(13):1864–73.
[14] O'Dwyer D. Funicular analysis of masonry vaults. Comput Struct 1999;73(1–5):187–97.
[15] Oppenheim IJ, Gunaratnam DJ, Allen RH. Limit state analysis of masonry domes. J Struct Eng ASCE 1989;115:868–82.
[16] Pesciullesi C, Rapallini M, Tralli A, Cianchi A. Optimal spherical masonry domes of uniform strength. J Struct Eng ASCE 1997;123:203–9.
[17] D'Ayala D, Casapulla C. Limit state analysis of hemispherical domes with finite friction. In: Lourenço PB, Roca P, editors. Proc. historical constructions, Guimarães PT; 2001.
[18] Roca P, Lopez-Almansa F, Miquel J, Hanganu A. Limit analysis of reinforced masonry vaults. Eng Struct 2007;29:431–9.
[19] Fangary AAH. Graphics analysis of gothic vaults. Master's Thesis Advanced Masters in Structural Analysis of Monuments and Historical Constructions, Springer, Berlin; 2010
[20] Block P, Ciblac T, Ochsendorf J. Real-time limit analysis of vaulted masonry buildings. Comput Struct 2006;84(29–30):1841–52.
[21] Creazza G, Saetta A, Matteazzi R, Vitaliani R. Analyses of masonry vaults: a macro approach based on three-dimensional damage model. J Struct Eng 2002;128(5):646–54.
[22] Creazza G, Saetta A, Matteazzi R, Vitaliani R. Analyses of masonry vaulted structures by using a 3-D damage model. European Congress on Computational Methods in Applied Sciences and Engineering, ECCOMAS 2000, Barcelona, SP; 2000.
[23] Vermeltfoort AV. Analysis and experiments of masonry arches. In: Lourenço PB, Roca P, editors. Proc. historical constructions, Guimarães PT; 2001.
[24] Faccio P, Foraboschi P, Siviero E. Masonry vaults reinforced with FPR strips [In Italian: Volte in muratura con rinforzi in FRP]. L'Edilizia 1999;7(8):44–50.
[25] Foraboschi P. Masonry structures externally reinforced with FRP strips: tests at the collapse [in Italian]. In: Proc. I Convegno Nazionale "Sperimentazioni su Materiali e Strutture", Venice; 2006.
[26] Fanning PJ, Boothby TE. Three dimensional modelling and full scale testing of stone arch bridges. Comput Struct 2001;79(29–30):2645–62.
[27] Fanning PJ, Boothby TE, Roberts BJ. Longitudinal and transverse effects in masonry arch assessment. Constr Build Mater 2001;15(1):51–60.
[28] Milani G, Lourenço PB. 3D non-linear behavior of masonry arch bridges. Comput Struct 2012;110–111:133–50.
[29] Milani G, Tralli A. A simple meso-macro model based on SQP for the non-linear analysis of masonry double curvature structures. Int J Solids Struct 2012;49(5):808–34.
[30] Milani G, Lourenço PB. Simple homogenized model for the non-linear analysis of FRP strengthened masonry structures. Part II: structural applications. J Eng Mech ASCE 2013;139(1):77–93.
[31] Milani G, Milani E, Tralli A. Upper Bound limit analysis model for FRP-reinforced masonry curved structures. Part I: unreinforced masonry failure surfaces. Comput Struct 2009;87(23–24):1516–33.
[32] Milani G, Milani E, Tralli A. Upper Bound limit analysis model for FRP-reinforced masonry curved structures. Part II: structural analyses. Comput Struct 2009;87(23–24):1534–58.
[33] Milani E, Milani G, Tralli A. Limit analysis of masonry vaults by means of curved shell finite elements and homogenization. Int J Solids Struct 2008;45(20):5258–88.
[34] Pippard AJS, Ashby ERJ. An experimental study of the voissour arch. J Inst Civil Eng 1936;10:383–403.
[35] Hughes TG, Blackler MJ. A review of the UK masonry arch assessment methods. Proc Instn Civil Eng 1997;122:305–15.
[36] Cavicchi A, Gambarotta L. Collapse analysis of masonry bridges taking into account arch-fill interaction. Eng Struct 2005;27(4):605–15.
[37] Cavicchi A, Gambarotta L. Two-dimensional finite element upper bound limit analysis of masonry bridges. Comput Struct 2006;84(31–32):2316–28.
[38] NTC 2008. Nuove norme tecniche per le costruzioni. Ministero delle Infrastrutture (GU n.29 04/02/2008), Rome, Italy, 14/01/2008.
[39] Circolare Esplicativa alle NCT 2008 n617 02/02/2009. Circolare n. 617 del 2 febbraio 2009 Istruzioni per l'Applicazione Nuove Norme Tecniche Costruzioni di cui al Decreto Ministeriale 14 gennaio 2008. Ministero delle Infrastrutture, Rome, Italy; 2009.
[40] Gilbert M. Ring: a 2D rigid block analysis program for masonry arch bridges. In: Proc. 3rd international arch bridges conference. Paris, France; 2001: p. 109–118.
[41] Gilbert M, Melbourne C. Rigid-block analysis to masonry arches. Struct Eng 1994;72:356–61.
[42] Gilbert M. Limit analysis of masonry block structures with non-associative frictional joints using linear programming. Comput Struct 2006;84:873–87.
[43] Milani G, Lourenco PB, Tralli A. Homogenised limit analysis of masonry walls. Part I: failure surfaces. Comput Struct 2006;84(3-4):166–80.
[44] Milani G, Lourenco PB, Tralli A. Homogenised limit analysis of masonry walls. Part II: structural examples. Comput Struct 2006;84(3–4):181–95.
[45] Milani G. Simple homogenization model for the non-linear analysis of in-plane loaded masonry walls. Comput Struct 2011;89:1586–601.
[46] Lourenço PB, Milani G, Tralli A, Zucchini A. Analysis of masonry structures: review of and recent trends in homogenisation techniques. Can J Civil Eng 2007;34(11):1443–57.